Locust Flight Muscle Activity and Body Orientation in Response to Objects Moving within Different Backgrounds

A Thesis Submitted to the College

of Graduate and Postdoctoral Studies

in Partial Fulfillment of the Requirements

for the Degree of Master of Science

in the Department of Biology

University of Saskatchewan

By

Sinan Zhang

© Copyright Sinan Zhang, April 2018. All rights reserved.

PERMISSION TO USE

In presenting this thesis in partial fulfillment of the requirements for a Postgraduate degree from the University of Saskatchewan, I agree that the Libraries of this University may make it freely available for inspection. I further agree that permission for copying of this thesis in any manner, in whole or in part, for scholarly purposes may be granted by the professor or professors who supervised my thesis work or, in their absence, by the Head of the Department or the Dean of the College in which my thesis work was done. It is understood that any copying or publication or use of this thesis or parts thereof for financial gain shall not be allowed without my written permission. It is also understood that due recognition shall be given to me and to the University of Saskatchewan in any scholarly use which may be made of any material in my thesis.

Requests for permission to copy or to make other uses of materials in this thesis in whole or part should be addressed to:

Head of the Department of Biology,

112 Science Place, University of Saskatchewan,

Saskatoon, Saskatchewan, Canada S7N 5E2

OR

Dean of College of Graduate and Postdoctoral Studies,

116 Thorvaldson Building, 110 Science Place, University of Saskatchewan,

Saskatoon, Saskatchewan, Canada S7N 5C9

ABSTRACT

Locusts are ideal model systems to study complex behaviours, such as flight responses to objects approaching on a collision course. Previous studies have described the flight muscle activity, wing kinematics and aerodynamic forces during collision avoidance behaviour of locusts flying in the wind tunnel. Neural recordings have revealed the influence of backgrounds on the responses of the descending contralateral movement detector (DCMD). Flow field backgrounds delay DCMD responses to looming stimuli that are known to evoke collision avoidance and muscle asynchrony during flight. **Therefore, I hypothesize that the flow field background will delay behavioural responses and affect the timing of flight muscle activity**. To test for this hypothesis, I placed a loosely-tethered flying locust inside a flight simulator, and presented visual stimuli composed of disks looming within different backgrounds. Concurrent electromyogram (EMG) and videos were recorded before and during the approach. My results show that against both simple and flow field backgrounds, the locust performed collision avoidance behaviours, by exiting the area defining the pre-response epoch, in most of the trials. The time of behaviour (TOB) varied among trials, and neither depressor asymmetry (DA) nor LM97 firing rate changed at TOB. The linear correlation between rotational degrees of freedom [RDOF, including roll (η), pitch(χ), and yaw(ψ)], or the changes in RDOF from the previous frame (ΔRDOF), and DA was calculated to investigate the relationship between depressor asymmetry and behaviours. In the presence of a simple background, more trials showed a significant correlation between RDOF and DA, compared to a flow field background. In the simple background,

the time when the correlation between RDOF/ΔRDOF (η, $\Delta\eta$, $\Delta\chi$, and $\Delta\psi$) and DA became significant occurred during the interquartile range of TOB. In the flow field background, the correlation between certain RDOF/ΔRDOF (η, ψ, $\Delta\eta$) and DA became significant, while the correlation between DA and χ became insignificant, during the interquartile range of TOB. These results suggest that the background types affected the correlation between RDOF (or ΔRDOF) and DA, and the time when the significance of the correlation changes could be related to TOB.

ACKNOWLEDGEMENTS

I feel very honoured to work with my supervisor, Dr. John Gray, and the wonderful colleagues in the Gray lab. Working in such a friendly environment has been a great pleasure. I would also like to thank my committee members, Dr. Tracy Marchant and Dr. Som Niyogi, for all their patience and help.

Thank you mom and dad, for the unconditional love and support you've been giving me over these years.

Thank you Basei, for the love and company.

TABLE OF CONTENTS

LIST OF FIGURES

LIST OF TABLES

LIST OF ABBREVIATIONS AND SYMBOLS

EMG	Electromyograph
DA	Depressor asymmetry
DCE	Double confinement ellipsoid
MVEE	Minimum volume enclosed ellipsoid
PPM	Pearson product-moment correlation
RDOF	Rotational degrees of freedom
TDOF	Translational degrees of freedom
TOB	Time of behaviour
TOC	Time of collision
WBF	Wing beat frequency
η	Roll
χ	Pitch
ψ	Yaw

CHAPTER 1. INTRODUCTION

1.1 NEUROETHOLOGY

In the natural environment, animals perform different kinds of behaviours in response to various biologically relevant stimuli. Neuroethology is the study of the neural basis of animal behaviours (Zupanc, 2010). It investigates how sensory organs process the environmental information, and how the central nervous system interprets the information to coordinate motor activities that produce the behavioural output observed under natural conditions (Zupanc, 2010).

Traditionally, neurobiologists have worked on anesthetized animals or isolated nervous tissues. Typically, the species is either chosen from established animal models, or systems that are tractable in the context of the neuroethological question. By contrast, ethologists often employ a whole-animal approach by studying the behaviour of an animal in its natural habitat, or conditions emulated in the lab which attempt to minimize disturbances by the experimenter.

Combinations of neurobiological and ethological approaches created a balance by which detailed neural function can be ascribed to natural behaviour. With the development of techniques, such as the focal brain stimulation technique invented by Walter Rudolf Hess (Hess, 2008), neurobiologists gradually founded a series of approaches and began to understand, from mechanistic and evolutionary perspectives, both specialization and diversity of neural control among different species (Huber, 1962; von Holst, 1939).

1.2 EXPERIMENTAL ANIMALS

Many advances in neuroethology came from studies using well-established animal models. Commonly used animals include bats (Griffin et al., 1960; Schnitzler and Flieger, 1983; Vater et al., 1995), zebra finch (Bottjer et al., 1984; Mello et al., 1995; Nottebohm et al., 1976), leopard frog (Ingle, 1973; King and Comer, 1996), mottled sculpin (Coombs, 1999; Dijkgraaf, 1963; Hoekstra and Janssen, 1985), noctuid moths (Coro and Perez, 1983; Roeder and Treat, 1957; Waters, 1996), etc., each has certain advantages in a specific research area.

For example, *Anolis carolinensis* (green anole) produces a set of behaviours in various social contexts including aggression, submission, and courtship (Greenberg and Noble, 1944). Complex but stereotyped, these behaviours have attracted many neuroethologists (Jenssen, 1971; Summers and Greenberg, 1995). Another species, *Petromyzon marinus* (sea lamprey), use an anguilliform mode of locomotion, and their nervous system is also quite robust, allowing long-term reduced-preparation experiments making it an ideal model to study the neural control of locomotion (Grillner, 1985; Rovainen, 1974; Vinay et al., 1996).

However, invertebrates, especially insects, are among the most attractive species to study in neuroethological research. Advantages include: ease of handling, inexpensive maintenance in laboratory conditions, as well as the tractability of their nervous system. For example, numerous attempts have been made to achieve flapping-wing flight since as early as the 9th century (White, 1961), yet few have succeeded (Helbling and Wood, 2017). The complex environments require flying animals to perform decisive and complicated aerial maneuvers, which require the ability to respond to salient cues in the

surrounding environment (Wilson, 1968). Vertebrate flight involves numerous neurons and muscles (Rayner, 1988), making it difficult to investigate at a cellular level. Compared to other flying animals, insects have a relatively tractable nervous system with fewer neurons involved in controlling complex movements (e.g. motor output can be directly related to behaviours) (Burrows, 1996). This attribute makes insects excellent experimental animals for the study of flight behaviours (Burrows, 1973).

In many species, specialized neural circuits named central pattern generators (CPGs) have been identified (Orlovskiĭ et al., 1999), which could produce rhythmic motor patterns without peripheral input. However, although CPGs do not require sensory feedback to be activated, the sensory information is necessary for the animals to generate appropriate behavioural responses. Therefore, the locomotion of the insects is constantly adjusted by both internal neural output and environmental feedback.

1.3 LOCUSTS

As the most widespread locust species, *Locusta migratoria* (Linnaeus, 1758) has also been commonly used in neuroethological studies. *L. Migratoria* belongs to the family *Acrididae* in the order Orthoptera. In response to changes in population density, it may transform between two main phenotypes, the solitary phase and the gregarious phase (Korzan et al., 2000; Pener and Yerushalmi, 1998). When population density increases, locusts transform from the solitary phase to the gregarious phase, changing in morphology and behaviours (Uvarov, 1977). In the solitary phase, locusts are nocturnal and cryptic: they tend to avoid other conspecifics, move slowly, and fly infrequently. Conversely, in the gregarious phase, locusts aggregate into swarms (up to 1,000

individuals per m^2), eat more, and fly frequently (mostly during the daytime) (Uvarov, 1977). This change is induced by an increase in the level of serotonin (Anstey et al., 2009), which is primarily caused by increased tactile stimulation on the hindleg over a four-hour period (Rogers et al., 2003; Simpson et al., 2001).

As a highly mobile species, locusts can fly with the wind at an average speed of 300 $cm \cdot s^{-1}$ (Baker et al., 1981). A locust swarm containing millions of individuals can cover up to several hundred km^2, and may travel more than 30 km a day (Simpson et al., 2007; Uvarov, 1966). An adult gregarious locust can consume its own weight of fresh food per day. This repeatedly causes huge losses in crops and therefore locusts are considered pests in many regions (Beĭ-Bienko and Mishchenko, 1963; Latchininsky et al., 2002; Tsyplenkov, 1970). In order to minimize their damage to agricultural production, scientists have been studying the biology of locusts for many years (Bate, 1976; Beĭ-Bienko and Mishchenko, 1963; Clynen et al., 2001; Loughton and Orchard, 1981; Mishchenko, 1952; Schoofs et al., 1993).

In flight-related neuroethological research, there are many advantages in choosing locust as the experimental animal. As insects, locusts are robust for electrophysiological experiments, easy to rear, and capable of producing rather complex long-term flight movements with a tractable nervous system. In addition, previous studies aiming at controlling locusts' population have provided a wealth of knowledge base on their general physiology, benefiting further investigation into their neuroethological characters.

1.4 LOCUST NERVOUS SYSTEM AND FLIGHT

Locusts possess a pair of compound eyes consisting of around 8,500 separate ommatidia, each with its own lens viewing 1.25° of the visual field (Horridge, 1978; Wilson, 1975; Wilson, 1978). Beneath each ommatidium are eight photoreceptors (retinula cells), all of which contribute to a single fused rhabdome (Wilson, 1978) (Figure 1.1).

Within the brain, the optic lobe of the locust is anatomically divided into three regions (distal to proximal): the lamina, the medulla and the lobula. Among the eight photoreceptors of each ommatidium, six project into the lamina, while the other two project into the medulla (Wilson, 1978). Neurons responding specifically to motion were first found in the medulla (James and Osorio, 1996; Osorio, 1986). However, the sizes of these neurons are so small that it is difficult to record from them. To date, motion-detecting neurons in the lobula have been best characterized (Gewecke and Hou, 1993; Gewecke et al., 1990; O'Shea and Williams, 1974; Rind, 1987; Rind, 1990a; Rind, 1990b).

Researchers have found several large fan-shaped neurons, one of which is the Lobula Giant Movement Detector (LGMD) (O'Shea and Williams, 1974). Together with its postsynaptic partner, the Descending Contralateral Movement Detector (DCMD) (O'Shea et al., 1974; Rowell, 1971), the LGMD responds to approaching objects, showing a rapid train of increasing action potential (spike) frequency during the approach (Rind and Simmons, 1992; Schlotterer, 1977; Simmons and Rind, 1992) (Figure 1.2).

Excitation of the LGMD begins when retinotopically arranged fibers within the ommatidia are stimulated by movement, and produce excitatory input onto one of the

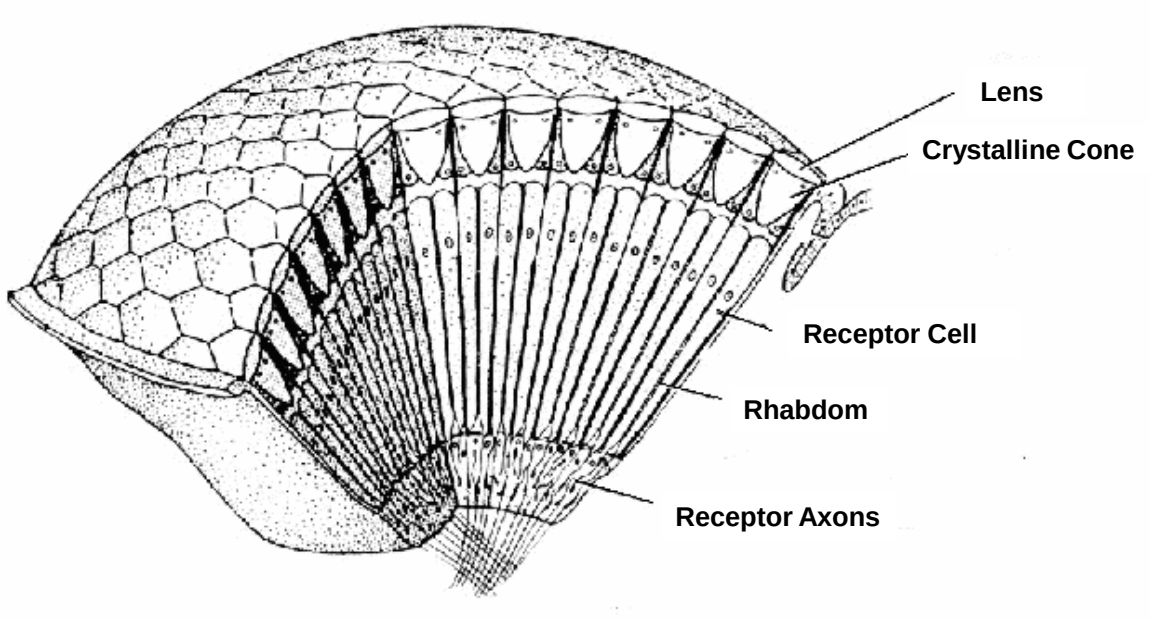

Figure 1.1 Schematic model of an apposition type of compound eye (Modified from Land and Nilsson, 2002).

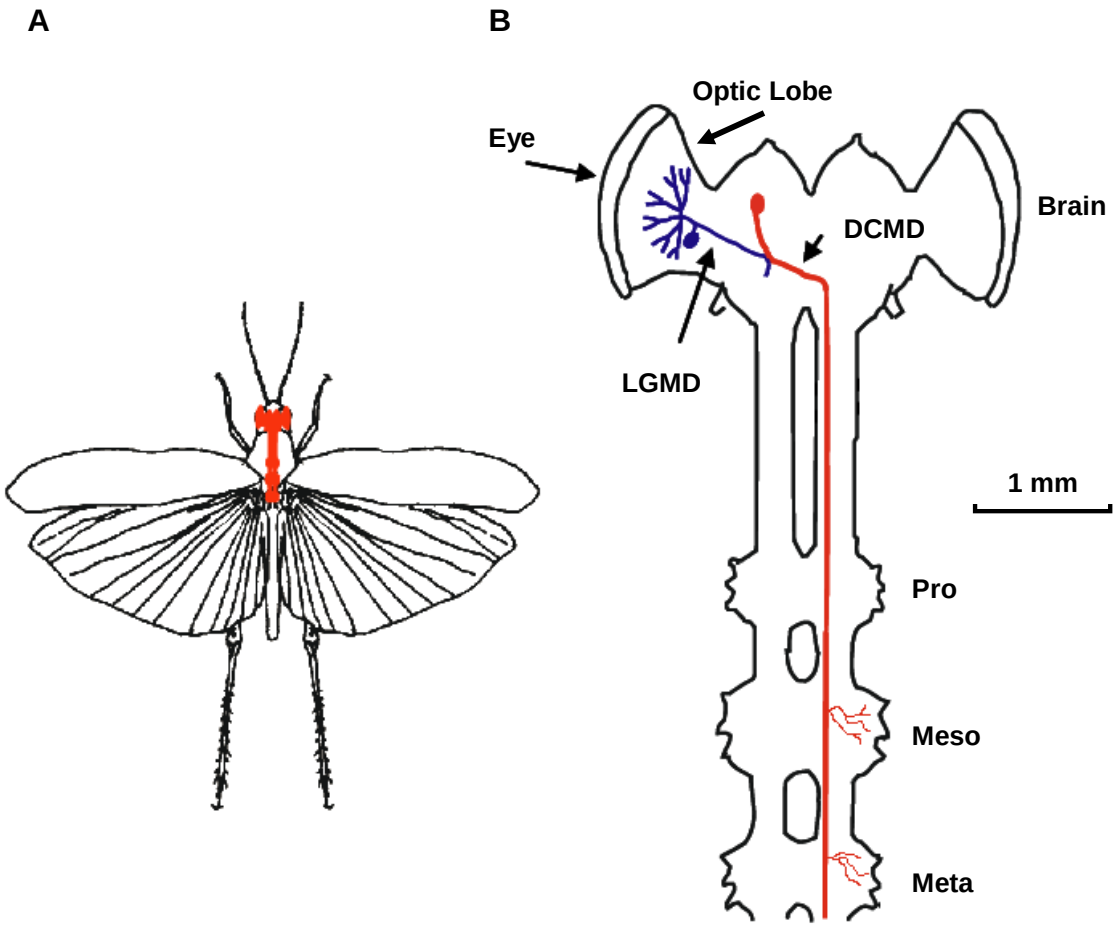

Figure 1.2 Diagram of the locust LGMD/DCMD pathway. A) Schematic of the locust body with scaled position of brain and thoracic ganglia in red. B) Enlarged view of the brain and thoracic ganglia. The Lobula Giant Movement Detector (LGMD) is situated the optic lobe of the brain and synapses onto the Descending Contralateral Movement Detector (DCMD). The DCMD axon crosses the midline of the brain, descends down the contralateral nerve chord, and branches within the meso- and metathoracic ganglia. Modified from McMillan (2009).

three large dendritic fields of the LGMD (Rind, 1984). During a looming approach (an object approaching along a direct collision course at constant velocity), the number of spikes produced by the LGMD is directly related to the approaching object's angular velocity and subtense angle and is thus referred to as an angular threshold detector (Gabbiani et al., 1999). The LGMD firing rate increases to a peak when an object approaches the retina, and decays once motion stops and before a collision would have occurred (Dick and Gray, 2014; Gabbiani et al., 1999; Gabbiani et al., 2001; Gabbiani et al., 2002; Gray, 2005; Guest and Gray, 2006; McMillan and Gray, 2012) (Figure 1.3). Presynaptic lateral inhibition and postsynaptic feed-forward inhibition from the other two LGMD dendritic fields control excitation and thus define the peak firing rate (Gabbiani et al., 1999; Gabbiani et al., 2001; Rowell and O'Shea, 1976). Each LGMD synapses onto a DCMD within the protocerebrum, generating a one-to-one spike ratio (O'Shea and Williams, 1974). In turn, DCMD descends along the contralateral side of the body and synapses with interneurons and motorneurons in the thoracic ganglia that control the wings and legs (Burrows and Fraser Rowell, 1973; Robertson and Pearson, 1983; Simmons, 1980). For the ease of access, many studies record from the DCMD axon within the contralateral side of the ventral nerve cord. A recent study utilizing principal component and dynamic factor analyses to investigate multichannel recordings from the DCMD revealed a more complex collision detection system than previously described (Dick et al., 2017), suggesting that more comprehensive studies are required to fully understand the motion detection system of the locust, especially during flight.

Locusts have two pairs of wings, controlled by ten muscles (Burrows, 1996). The forewings are located on the mesothoracic segment, while the hindwings are on the

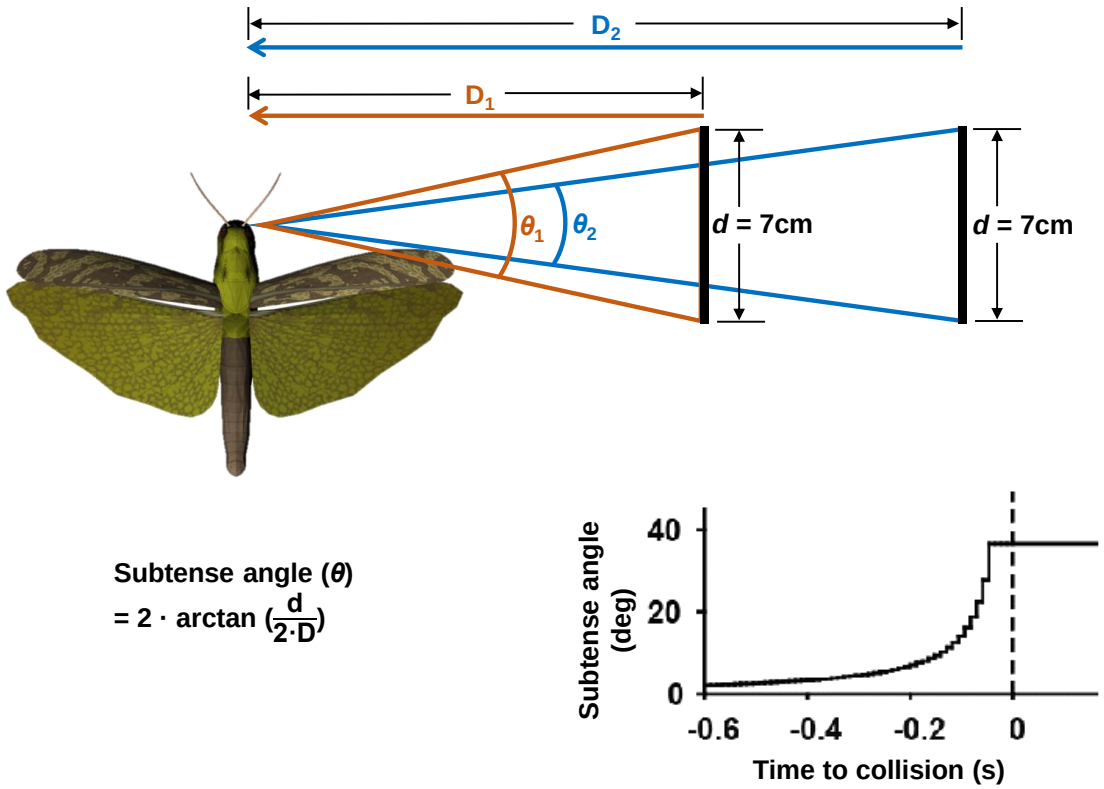

Figure 1.3 Schematic showing the subtense angle (θ) of disc at two distances from the locust eye. As the disc approaches, the angle subtended increases. The inset on the bottom right shows the subtense angle during an approach of a computer-generated disc approaching at constant velocity (300 cm·s^{-1}). Modified from McMillan (2009).

metathorax (Wilson, 1968) (Figure 1.4). The anatomical structure and the function of the two pairs of wings are not the same. With a larger surface, the hindwings offer most of the lift; while the forewings, comparatively more rigid, generate steering movements (Dawson et al., 1997). The average wing beat frequency, varying among sex, size and temperature, is 23 Hz (Baker et al., 1981). The ten muscles either attach directly to the base of the wings or cause wing movements indirectly by deforming the thoracic box (Shoemaker and Robertson, 1998). Electromyographic (EMG) recordings from these muscles have revealed a stereotyped pattern of muscle contractions during flight, which is termed the flight motor pattern and consists of alternating activity in elevator and depressor muscles of the wing (Wilson and Weis-Fogh, 1962).

Different wing movements are controlled by changes in the timing and strength of the contraction of particular wing muscles. For example, the relative timing of the forewing first basilar depressor muscle (M97), which shows an earlier firing by 10-15 ms on the inside of turning, is used as an accurate indicator of steering (McMillan et al., 2013; Wilson and Weis-Fogh, 1962). During straight flight, the firing time of M97 on both sides is similar. During a left turn, for example, the left M97 fires earlier, terminating the elevation of the left forewing earlier and resulting in lower left wingbeat amplitude. As a result, there is reduced rotational torque on the left side, resulting in a left turn. Complete steering behaviour requires coordinated responses of the abdomen, hindlegs, and wings (Robertson and Johnson, 1993). A change in forewing asymmetry is the most consistently observed reaction, and is strongly affected by the speed and size of an approaching target. This suggests that a collision avoidance maneuver may depend more on these aspects of the reaction (Robertson and Johnson, 1993). The result of these

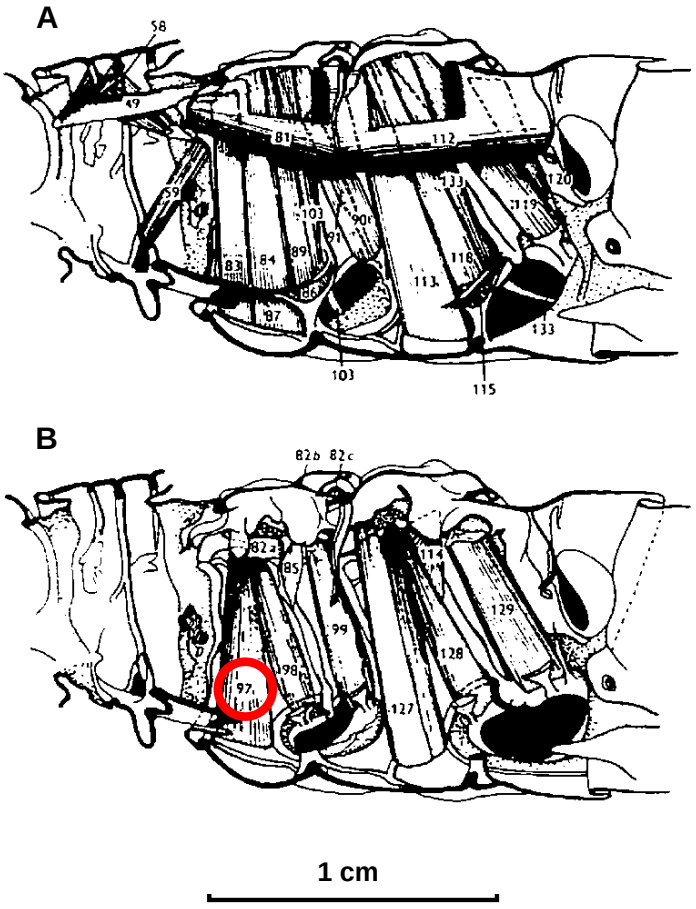

Figure 1.4 Locust mesothoracic and metathoracic flight musculature. **A.** Elevator muscles. **B.** Depressor muscles (Wilson and Weis-Fogh, 1962). A total of 10 pairs of muscles are involved in locust flight control. These muscles either attach directly to the base of the wings or cause wing movements indirectly by deforming the thoracic box. The forewing first basalar depressor muscle (M97) is labeled with a red circle. M97 asymmetry has often been used as an indicator of flight steering of locusts.

steering responses can be the movement of the body in any of the three rotational degrees of freedom [roll(η), pitch(χ), yaw(ψ)] or the three translational degrees of freedom (thrust, sideslip, or lift) (Baker, 1979; McMillan et al., 2013) (Figure 1.5). The combination of these movements results in the directional orientation of the insect in flight.

1.5 METHODOLOGICAL APPROACHES

Numerous methodological approaches, including those from traditional ethological research and those from, relatively, modern neurobiological research, have been developed to study collision avoidance behaviours of locusts. In collision avoidance studies, artificial stimuli and electrophysiological recordings are the most popular approaches.

Artificial stimuli have been widely adopted in biological studies. By extracting salient elements of the natural stimuli and reproducing them in the lab, researchers managed to record the animal's reactions under precisely controlled conditions. Specific to collision avoidance behaviours, it has been found that the velocity of edge expansion is a critical cue for locusts to detect an approaching or receding object (Chan and Gabbiani, 2013; Fotowat et al., 2011; Gray et al., 2001; Robertson and Johnson, 1993; Robertson and Reye, 1992; Santer et al., 2005; Simmons et al., 2010). Therefore, looming stimuli, varying in velocity of edge expansion, have been widely adopted in these studies.

In order to imitate the view of the locust during natural flight, a flight simulator has been developed (Gray et al., 2002). By placing the locust at the centre of a dome-shaped rear projection screen, which occupies 270° of the locust's view, and projecting

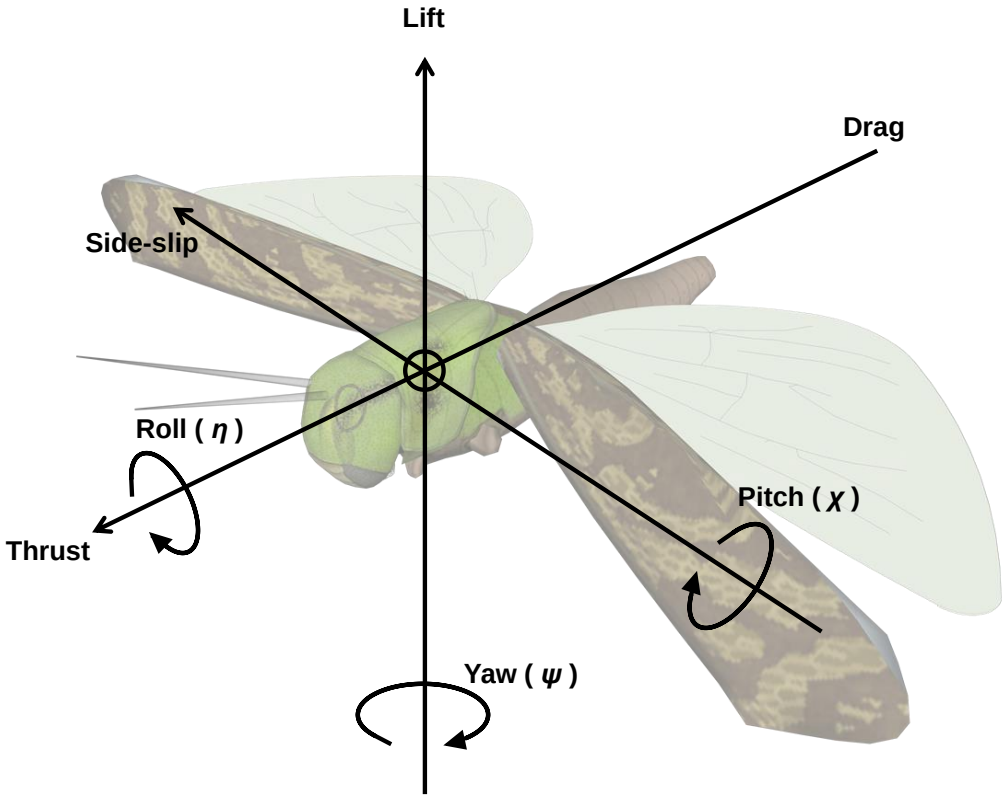

Figure 1.5 Diagram illustrating the three rotational degrees of freedom [roll(η), pitch(χ), yaw(ψ)] and the three translational degrees of freedom (thrust/drag, side-slip and lift) of a flying locust.

onto the screen, the flight simulator makes it possible to present visual stimuli and record the locust's responses simultaneously.

Previous studies used head-on wind flow at a speed of 300 $cm \cdot s^{-1}$, which is the same as the average locust flight speed (Baker et al., 1981), to induce long flight duration (Robertson and Johnson, 1993). While a loosely-tethered set up has been developed which allows locust flight motion in 3 dimensions, these experiments were conducted in a wind tunnel (McMillan et al., 2013). Since the visual stimuli can only be projected from the side, the wind tunnel precluded the use of complex visual stimuli that are available in the flight simulator.

Electromyographic (EMG) recording is one of the most widely employed approaches in neuroethological studies. By implanting electrodes into identified muscles, researchers are able to record and evaluate the electrical activities initiated by the nervous system. Two types of muscles, neurogenic (impulse originates in nervous system) and myogenic (impulse originates in muscle or modified "specialized" muscle tissue), have been found in insects. Because of the difference in impulse origins, myogenic muscles do not reflect individual spikes of motorneurons, while neurogenic muscle contractions are induced by individual action potentials from motorneurons. The wing movements of the locust have been found coordinated by the central nervous system and are, thus, neurogenic (Wendler, 1974; Wilson, 1961). About 80 motorneurons, controlled by numerous interneurons located in the thoracic ganglia, have been identified to be active during flight rhythm (Meldrum Robertson, 1986). These motorneurons have been categorized into two homologs that control the forewings and the hindwings, respectively.

1.6 PROGRESS AND CONCEPTION

Thus far, flight muscle activity, wing kinematics and aerodynamic forces of locusts have been recorded during collision avoidance behaviour and measured from rigidly-tethered locusts flying in open-loop conditions (Gray et al., 2001; Hedwig and Becher, 1998; Ribak et al., 2012; Robertson and Johnson, 1993; Robertson and Reye, 1992; Santer, 2006; Santer et al., 2005; Simmons et al., 2010). However, loosely-tethered flying locusts are capable of changing orientation in response to looming stimuli within a single wing beat (Mohr and Gray, 2003), and generate avoidance responses within a single downstroke (Ribak et al., 2012). To obtain a deeper understanding into locust flight, it is necessary to allow the animal to manoeuvre in 3-dimensional space in closed-loop conditions. Compared to the open-loop setup, in which the environmental conditions (e.g. artificial visual stimuli) are not dependent on the response of the animal, the closed-loop setup takes feedback from the behavioural output of the animal and adjusts the environmental conditions accordingly. Thus, we could continuously observe the long-term behaviours of the locust, instead of only the initial response.

Using a minimally restrained preparation, Chan and Gabbiani (2013) observed several behaviours, including wing kinematics and body rotations, which have been shown or indicated in rigidly tethered preparations. McMillan et al. (2013) used a combination of EMG recordings and motion analysis on loosely-tethered flying locusts in a wind tunnel, and showed the relationships between forewing depressor muscle activity, wing kinematics and 3-dimensional body responding to lateral looming visual stimuli. With a similar set-up, Manchester and Gray (in preparation) investigated the timing and

synchrony of multiple flight muscle activities, correlating them with wing kinematics and whole-body motion.

A flow field background, which mimics the optic flow produced during locust flight, was applied to investigate the effect of visual background on collision detection circuits. In rigidly-tethered locusts, the presence of flow field background caused reduced firing rates, delayed peaks, shorter rise phases, and longer fall phases in DCMD responses. Spike numbers were also reduced in the flow field background (Figure 1.6) (Silva et al., 2015).

However, behavioural responses of loosely-tethered locusts presented with more complex visual stimuli had not been investigated. Flow field backgrounds delay DCMD responses to looming stimuli that are known to evoke collision avoidance and muscle asynchrony during flight. **Therefore, I hypothesize that the flow field background will delay behavioural responses and affect the timing of flight muscle activity**. To test for this hypothesis, we constructed an air delivery system inside the flight simulator, which allowed us to place a loosely-tethered locust inside the flight simulator and initiate loosely-tethered flight. With this set-up, it is now possible to present complex visual stimuli in conjunction with EMG and video recordings. Since this set-up mimics the natural environment of the locusts better than the wind tunnel, it provides a new perspective of investigating how the flying locusts perform collision avoidance behaviours in the real world.

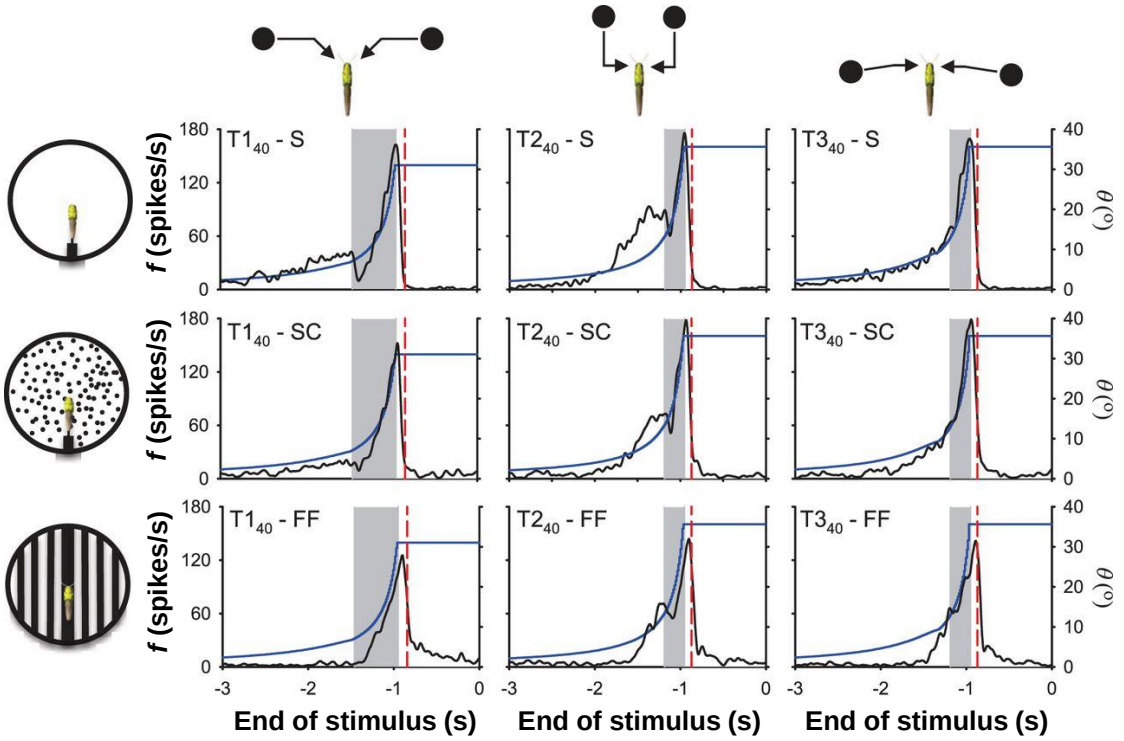

Figure 1.6 Effects of background complexity on the averaged Descending Contralateral Movement Detector (DCMD) responses of locusts (N = 28). Three compound trajectories composed of two disks transited from non-looming to looming were presented to each locust with three different backgrounds: simple (S), scattered (SC), and flow field (FF). Grey shading represents the looming phase of the stimulus (subtense angle shown with blue line), while the red dashed line represents the time of collision (TOC). As shown in each column, compared to the simple background, the presence of the flow field background caused delayed peaks, lower peak firing rate, shorter rise phases, and longer fall phases in all three trajectories. (Silva et al., 2015).

CHAPTER 2. MATERIALS AND METHODS

2.1 ANIMALS

Twenty adult male *Locusta migratoria* were selected at least 3 weeks past the imaginal moult from a colony (~30 °C, 12 h:12 h light: dark cycle) maintained at the University of Saskatchewan, Saskatoon, Canada. Experiments were carried out at room temperature (~25 °C) during similar times of the animals' light cycle to eliminate potential variation in responsiveness known to occur when the locusts fly at night. The colony was maintained crowded to ensure the animals were in gregarious state (Gaten et al., 2012).

2.2 PREPARATION

The locust's legs were removed to prevent the EMG electrodes from being dislodged (Robertson et al., 1996). A 3D-printed 2-cm-diameter ring connector was mounted onto the dorsum of the pronotum using low melting point beeswax and then the locust was rotated ventral side up. A pair of single 100 µm fine copper electromyographic (EMG) wires (Belden, St Laurent, QB, Canada) that were insulated except at the tip were inserted into the left and right M97 (forewing first basilar depressor muscles) which associate with attempted steering manoeuvres in rigidly tethered locusts (Dawson et al., 1997; Dawson et al., 2004; McMillan et al., 2013; Möhl and Zarnack, 1977; Shoemaker and Robertson, 1998; Zarnack, 1988). A ground wire was inserted slightly off the midline of the mesothoracic sternum. The EMG and ground wires were fixed to the locust's exoskeleton with low melting point beeswax (Figure 2.1A).

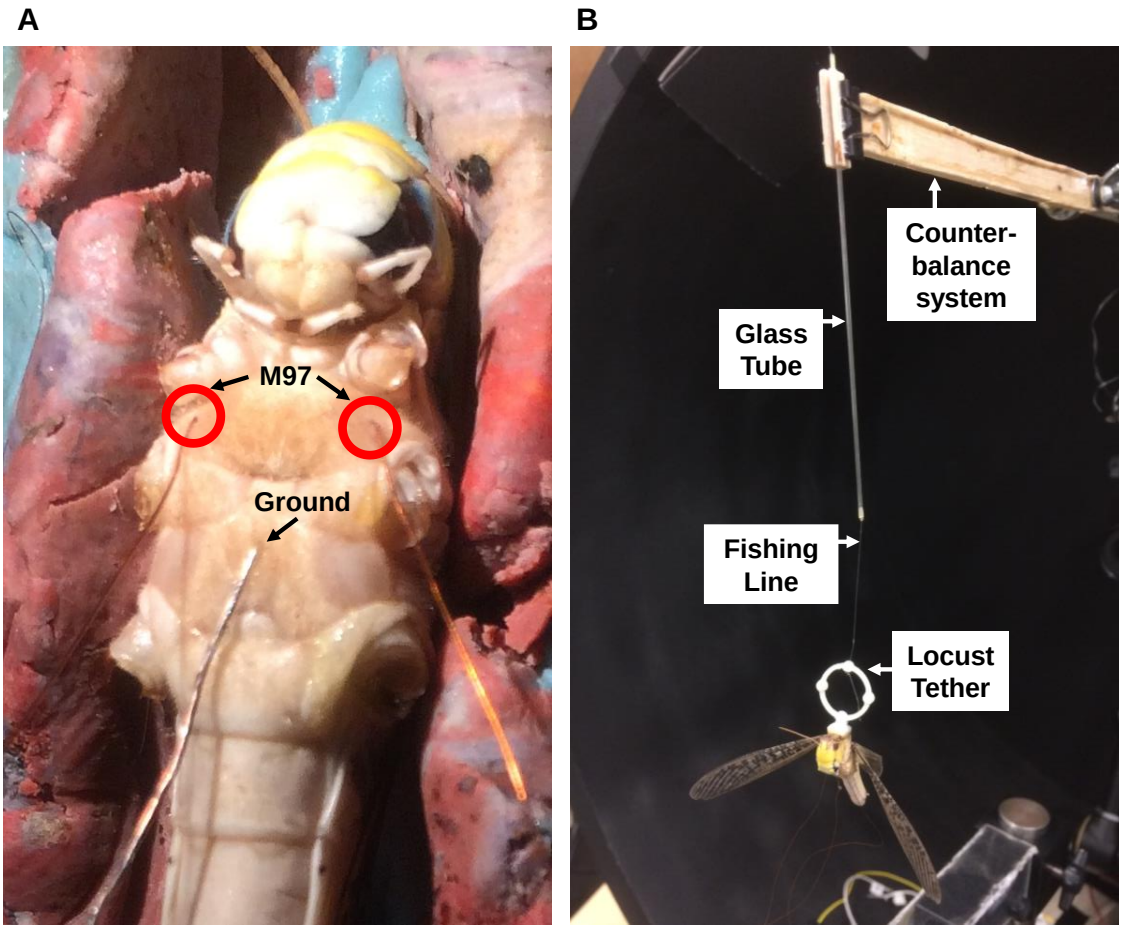

Figure 2.1 Photo of the EMG electrodes insertion sites and the tether. **A.** Photo showing the two wire electrodes (cooper) inserted into left and right M97. The silver wire in the middle is the ground wire. **B.** Photo showing a locust suspended on the counter balance system. The fishing line that connects to the tether was restricted by a piece of glass tube in order to limit the trajectory of the locust within the area of wind supply.

The tether consisted of 30 cm of 0.2 mm diameter clear fishing line (Berkley Trilene XT Extra Tough Line, Pure Fishing, Columbia, SC, USA) that was threaded through a piece of glass capillary tube, leaving approximately 3 cm free on the bottom (Figure 2.1B). This restricted the locust's flight within a relatively small three-dimensional (3D) volume of space that was appropriate for wind delivery and the field of view of the cameras. The total weight of the tether, including the beeswax, the glass tube and fishing line, was approximately 0.3 g. One end of the fishing line was mounted on a counter-balance system, which cancelled out the weight of the tether, allowing the locust to fly while carrying only its own body weight. The other end was attached to the top of the ring connector with four markers at the top, left, right, bottom quadrants (Figure 2.1B). These markers were subsequently used as references in 3D motion tracking.

The locust was suspended in the center of a flight simulator (Gray et al., 2002) (Figure 2.2) with the azimuthal and elevation axes of the apex of the rear projection dome screen 24 cm away. In this orientation, 0° was directly in front of the locust, left 90° was the center of the left eye, and right 90° was the center of the right eye. Wind flow was provided in a cylinder-shaped area by a colourless propeller mounted 10 cm in front of the locust. Wind speed was set to 300 $cm \cdot s^{-1}$, as measured with a hot-wire anemometer (VWT Scientific, Edmonton, AB, Canada), which is consistent with a locust's average flight speed (300-600 $cm \cdot s^{-1}$) (Baker et al., 1981). The volume of the space with wind supply was approximately 6,000 cm^3. Room lights were turned off during the experimentation. The setup was illuminated with an infrared light mounted behind the animal. The infrared could be recorded by the cameras, yet did not affect the locust's behaviours since it is beyond the spectral sensitive of the locust (Bennett et al., 1967).

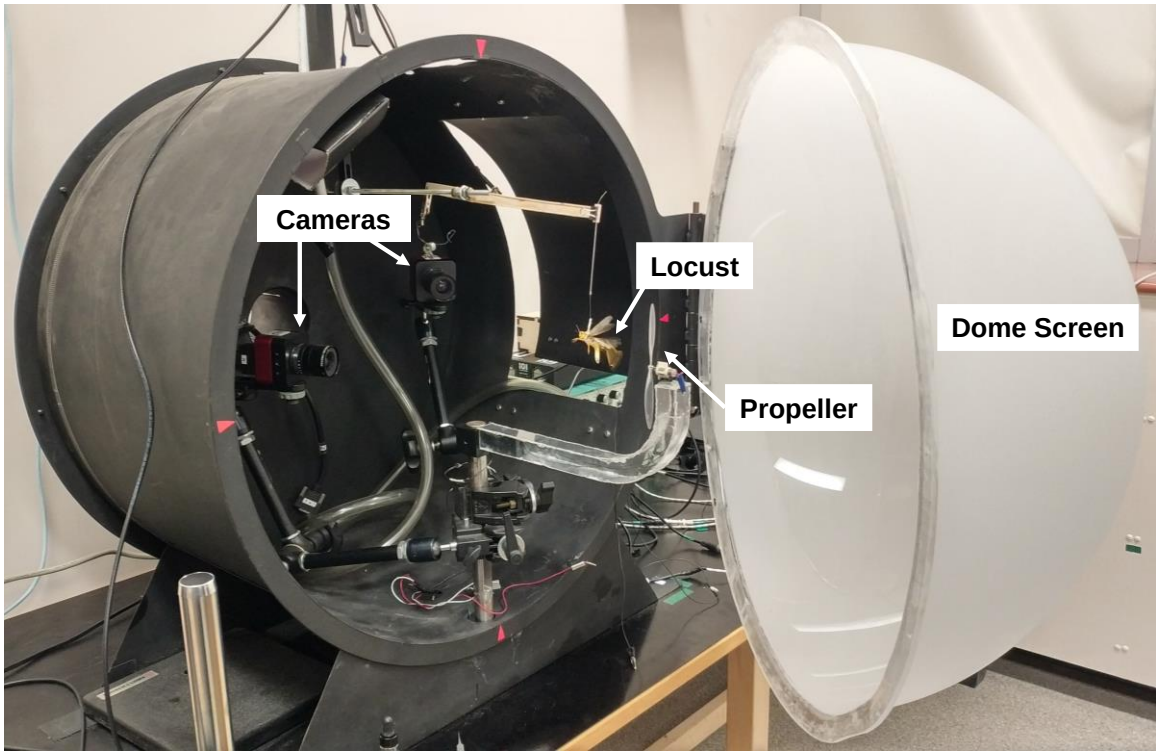

Figure 2.2 Photo of the flight simulator with the air delivery system. The locust was suspended in the center of the dome when the dome screen is closed. The colourless propeller could provide head-on wind supply to maintain the locust flight. Two cameras were mounted in the back to record the flight trajectory and body orientation of the locust.

2.3 VISUAL STIMULI

Visual stimuli began once the locust maintained >1 min of stable flight within the wind flow. During stable flight, the locust's position deviated ±1.5 cm in the x-axis, ±1 cm in the y-axis, and ±1.5 cm in the z-axis from its average position. The stimulus was generated using Vision Egg (Straw, 2008) on a Python programming platform (Python Software Foundation, https://www.python.org/) and represented as 1024×1024-pixel portable network graphics (png) files. Images were projected onto a rear projection dome screen at 85 frames·s^{-1} using a Sony projector (VPL-PX11 LCD video projector, Sony of Canada Ltd., Toronto, ON, Canada). This is above the mean flicker fusion frequency of the locust's eye (66.3 Hz) (Miall, 1978). The scaling factor for each frame was calculated to emulate nonlinear edge expansion produced by a looming object, and embedded into the Vision Egg code. Each pixel on the screen was ~0.7 mm, which subtends approximately 0.4° visual subtense angle on the locust's eye. This is below the 1° resolution of individual ommatidia (Horridge, 1978). Pixels near the edge of the dome screen would likely extend beyond the resolution of an individual ommatidium, due to the distortion by the curvature of the dome. However, those pixels constituted part of the white background, and thus did not affect the resolution of the moving objects. The luminance values (L_H = 483 cd·m^{-2} for the background and L_L = 170 cd·m^{-2} for the disk) and Michelson contrast ratio ($C_M = (L_H-L_L)/(L_H+L_L)$ = 0.48) were similar to those used by previous studies (Dick and Gray, 2014; Gray, 2005; Guest and Gray, 2006; McMillan and Gray, 2012).

All visual stimuli were presented at 0° elevation within the azimuthal plane (Figure 2.3). Each loom consisted of a 7-cm diameter black disc starting at a virtual

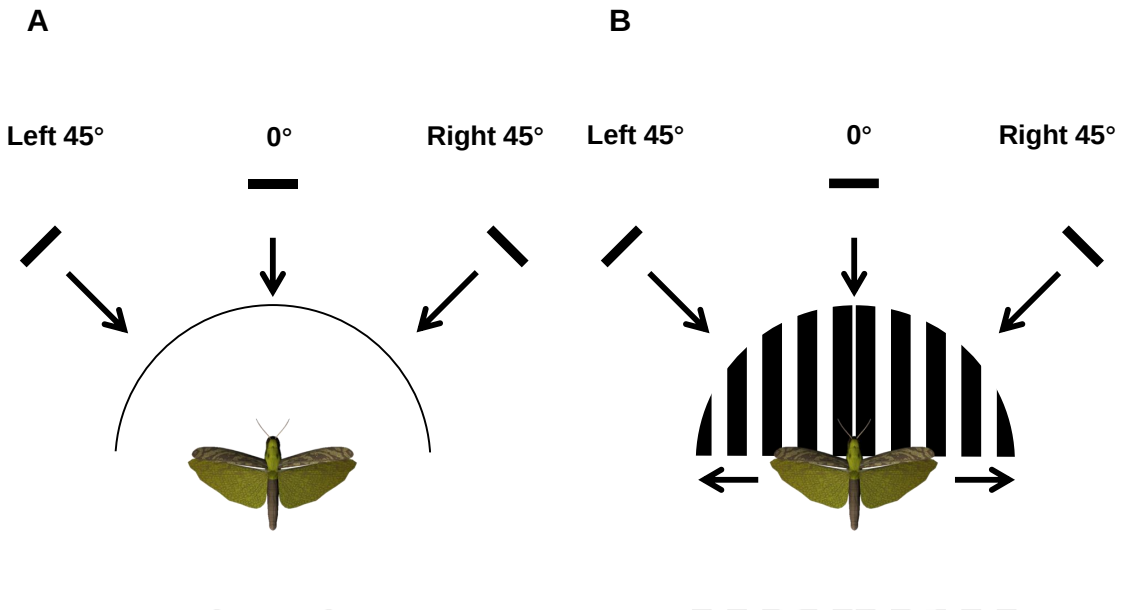

Figure 2.3 Diagram of the top view of the locust and screen (not to scale). **A.** The simple background (S). **B.** The flow field background (FF), composed of vertical bars moving outwards in the azimuthal plane from the dome apex. Looming stimuli (black discs) approached from left or right 45° in the azimuthal plane. Before every series of looming stimuli, a frontal loom (0° azimuth) was presented.

distance of 600 cm, travelling at a constant speed of 300 $cm \cdot s^{-1}$ on a direct collision course with the locust. The initial subtense angle was 0.67°. The initial and final approach trajectory was a frontal looming disk (0° azimuth), which was used to evaluate the general responsiveness of each locust. After the initial loom, a series of 4 visual stimuli was presented to each locust: disk approaching from left or right at 45° azimuth in the locust's frontal visual field against two background types (total of 80 approaches in the dataset). The order of looms was randomized for each locust. The simple background (S) was a white background with no object motion other than the 7-cm disk. The flow field background (FF) consisted of a modified vertical grating pattern that composed of vertical bars (width of each bar = 2 cm; angular size = 11.42°) moving outwards in the azimuthal plane from the dome apex. Each bar moved at a speed of 13.8 $cm \cdot s^{-1}$ across the dome and extended across the entire vertical height of the dome screen before disappearing at the edge of the dome. The background maintained a similar contrast ratio (0.48) with the object and the properties of the flow field were consistent with previous studies (Silva et al., 2012; Silva et al., 2015).

Based on the position of the locust during stable flight, the projected time of collision (TOC) was calculated. The 3D deviation of the locust's position during stable flight would produce a variation in the TOC of ±10 ms, which is relatively brief compared to the entire course of object motion (2,000 ms). Therefore, TOC was calculated from the average coordinates of the locust during the stable flight. Since the movement of the object could be seen in the videos (4 $ms \cdot frame^{-1}$), the frame in which the disk stopped expanding was identified. The distance between the locust and the dome

apex was 24 cm, and the disk was travelling at 300 cm·s^{-1}, therefore TOC would be 80 ms after that frame (Figure 2.4).

2.4 RECORDING

Flight behaviours were recorded with two monochrome digital cameras (Flare, IO Industries, London, ON, Canada), located behind the locust and 45 degrees to either side of the longitudinal axis. Each camera, recording 900×900 pixels at 250 frames·s^{-1}, was connected to a digital video recorder (Express DVR, IO Industries, London, ON, Canada). The recordings were exported to the computer after each trial. EMG data were recorded continuously using two channels of an A/D converter (National Instruments, Vaudreuil-Dorion, QB, Canada) recording at 25,000 Hz, and captured with LabVIEW (National Instruments Corporation, Austin, TX, USA) (Figure 2.5).

To align the videos and EMG data with TOC, a trigger was embedded into the recordings. EMG recording was first started manually, and the trigger was pressed subsequently. This would initiate video recordings, and simultaneously generate a square-wave pulse in a separate channel along with the EMG recordings. This pulse was used to align both recordings with TOC.

2.5 DATA ANALYSIS

Video files were imported into WinAnalyze3D motion analysis software (Mikromak, Berlin, Germany), which was calibrated for 3-dimensional measurements using a 43-point calibration frame (Figure 2.6). The videos were first examined to determine the time of behavioural changes. Subsequently, a 3D motion tracking of the

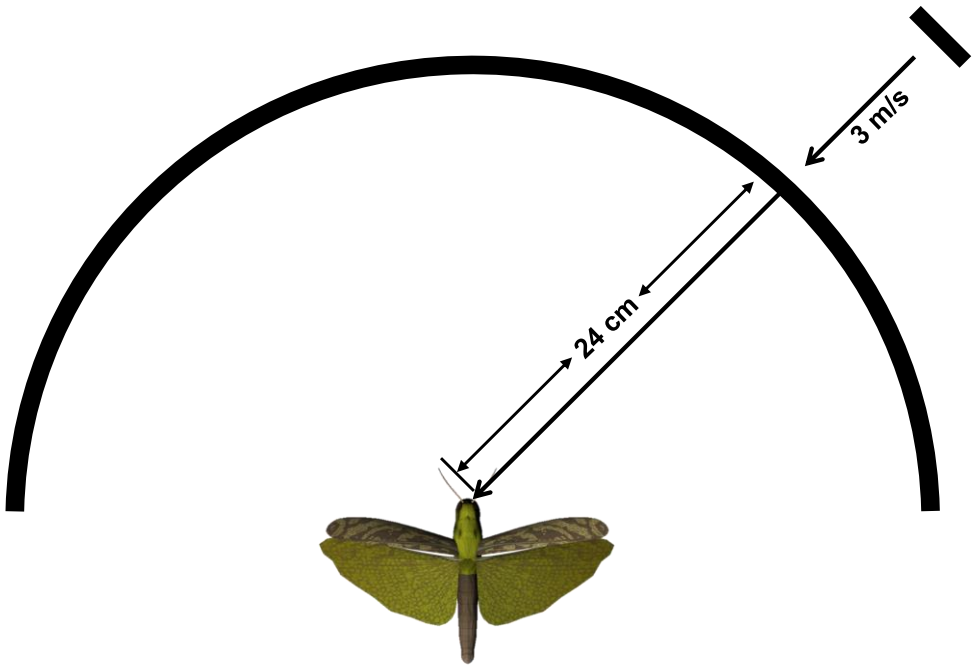

Figure 2.4 The estimation of the time of collision (TOC). As shown in the diagram, the locust (top view) was placed in the center of the dome (not to scale). The average distance between the dome and the locust compound eye was approximately 24 cm. The looming stimulus approached at 300 $cm \cdot s^{-1}$, and thus the projected TOC would be 0.08 seconds after the object stopped moving. The 3D deviation of the locust's position during stable flight would produce a variation of ±10 ms in the TOC, which is relatively brief compared to the entire course of object motion (2,000 ms). Therefore, TOC was calculated from the average coordinates of the locust during the stable flight.

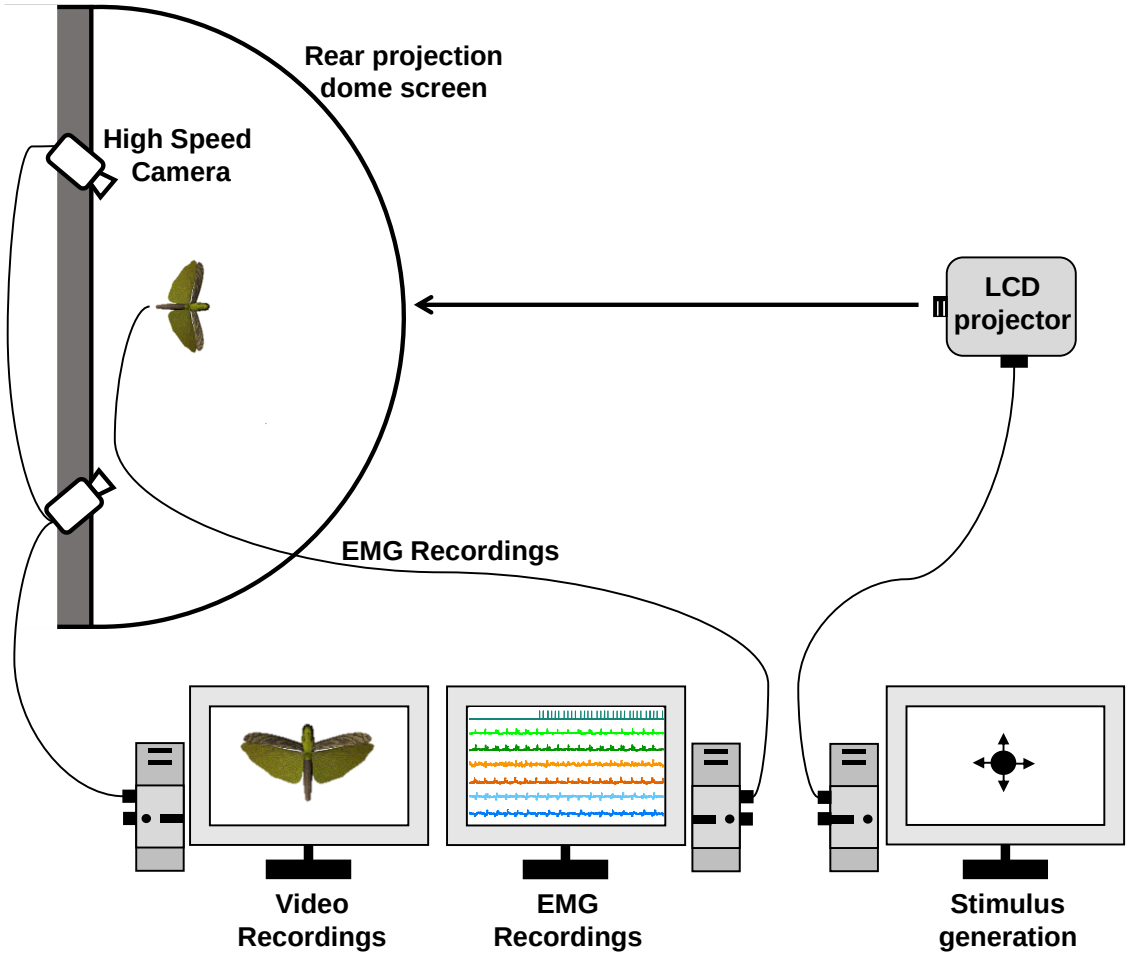

Figure 2.5. Diagram of the experimental setup. Vision egg ran on the stimulus generation computer, which was connected to a LCD projector that projected the visual stimuli onto the dome screen. Concurrent electromyographic (EMG) signals and high-speed videos were recorded separately on different computers. A trigger pulse was used to align EMG and video recordings, and the image of the looming object was used to calculate the time of collision (TOC) (shown in Figure 2.4).

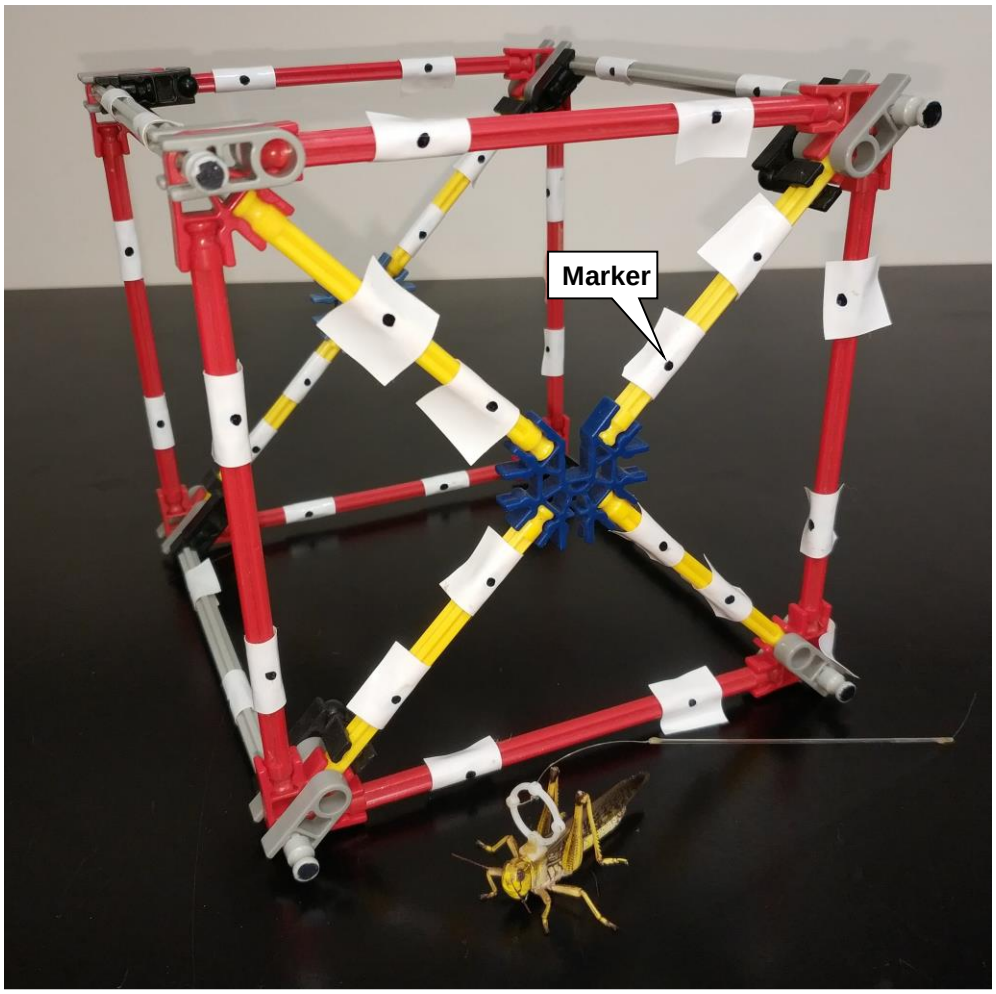

Figure 2.6 The calibration frame used in three-dimensional (3D) motion tracking. A total of 43 markers were labeled on the calibration frame, and the 3D coordinates of these markers were measured in a right-handed coordinate system. With two cameras recording simultaneously, the cameras' position could be calibrated, and thus we could extract the 3D locations of the locust tether during the recording. A locust was used as a reference of scale.

tether was performed, and the *x*-, *y*- and *z*-coordinates of the four markers were then exported for further analysis.

To quantify the collision-avoidance behaviour, a confinement ellipsoid (minimum volume enclosed ellipsoid, MVEE) (Moshtagh, 2005) was first computed in Matlab R2016a (Mathworks, Natick, MA, USA) for each trial. MVEE was the smallest ellipsoid around the cloud of points representing the flight trajectory of the subject during free flight. Previous studies (Benaragama and Gray, 2014; Chan and Gabbiani, 2013; McMillan et al., 2013) have found that locusts usually responded to looming object 0.84 s before collision, which translates into subtense angles of about 1.5°. Therefore, data from 2 to1 seconds before TOC were defined as the pre-response epoch, and was used to calculate the MVEE. Because of the corrective steering, the MVEE of each trial was not the same, and thus they were calculated individually. The exit point of the collision-avoidance behaviour was defined as the point at which the trajectory exited an ellipsoid twice the scalar dimensions of the one computed above (doubled confinement ellipsoid, or DCE) (Chan and Gabbiani, 2013). The turning angle between each frame was calculated. If the angle is $\geq 90°$, the animal was considered flying along the same course, while an angle $< 90°$ indicates a sudden change in flight trajectory. Therefore, the last frame in which the locust made a sharp turn ($< 90°$) before exiting DCE was defined as the time of behaviour (TOB) (Figure 2.7).

The coordinates from the four markers were then used to calculate the rotational degrees of freedom [RDOF, roll (η), pitch (χ) and yaw (ψ) angles] of the locust flight during the loom (Figure 2.8). η was calculated from the *x*- and *y*- coordinates for the top (*t*) and bottom (*b*) marker of the tether, where b_x is the x-coordinate of the bottom marker,

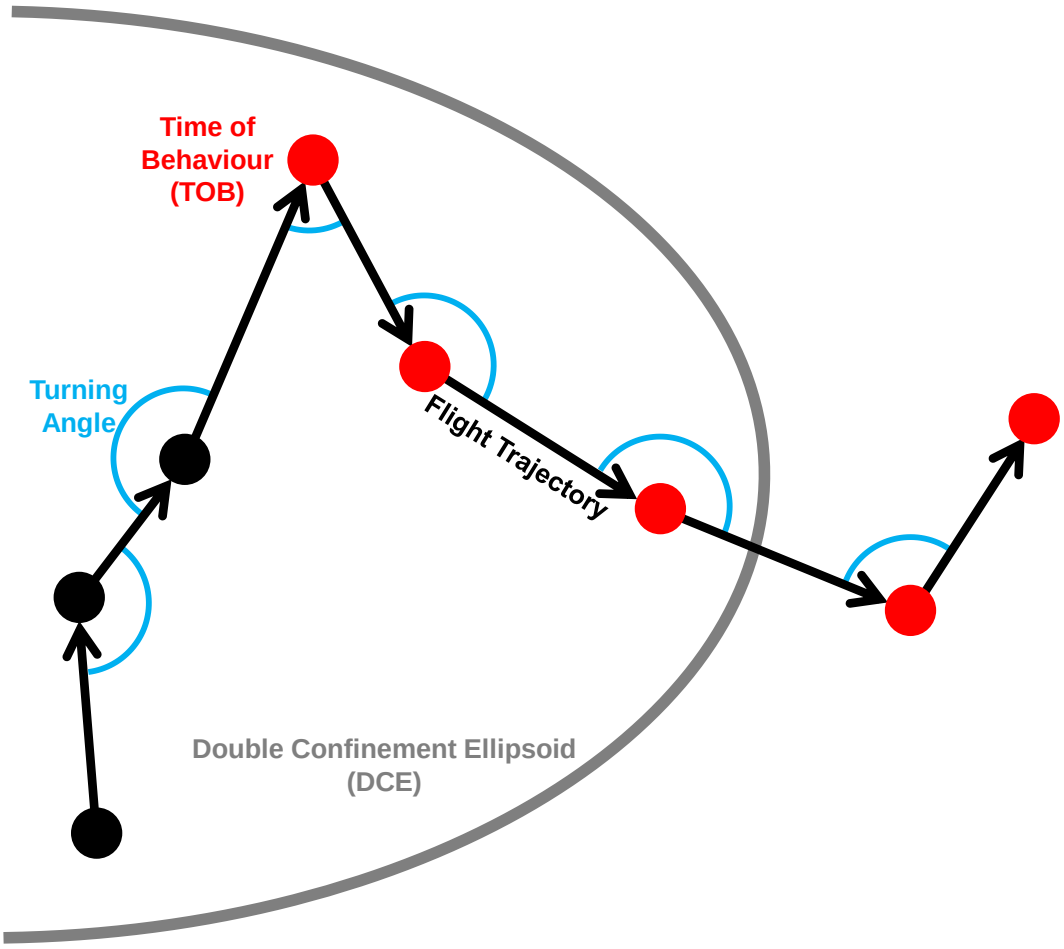

Figure 2.7 Simplified diagram demonstrating the calculation of the time of behaviour (TOB). The grey arc represents a portion of the double confinement ellipsoid (DCE) defining the pre-response epoch of the locust. The black arrows represent the flight trajectory (shown in 2 dimensions), while the black and red dots represent the location of the locust at each frame. The last frame in which the locust made a sharp turn (<90°) before exiting the DCE was defined as the TOB. The turning angle at each frame (blue arc) was calculated as the interior angle of the triangle defined by the location of the locust in three successive frames, and thus it is always between 0° and 180°. The positions after TOB are labeled red.

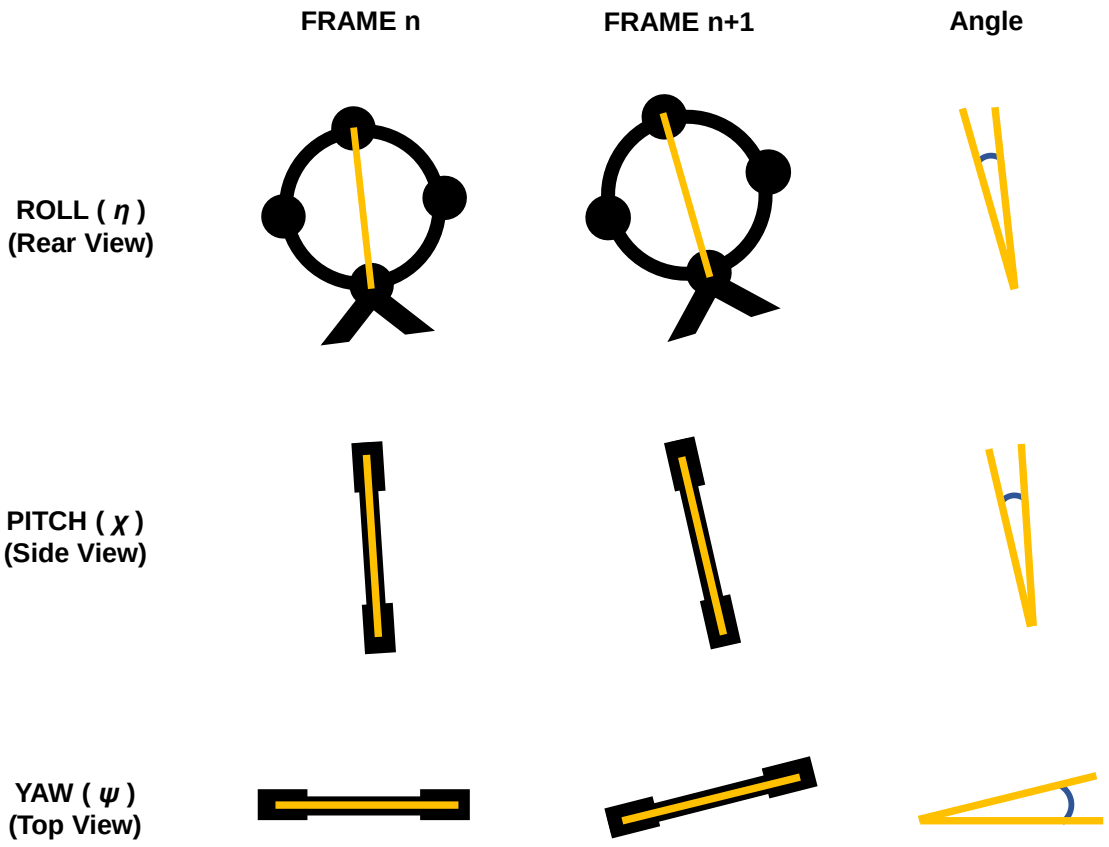

Figure 2.8 Diagram demonstrating the calculation of rotational degrees of freedom (RDOF). The images in the 1st and 2nd columns show the position of the tether in two successive frames. The yellow bar connects top and bottom marker. By subtracting the coordinates of these two markers in frame n from those in frame (n+1), we determined the angle shown with the blue arc in the 3rd column, representing the change of RDOF between the two frames.

b_y is the y-coordinate of the bottom marker, t_x is the x-coordinate of the top marker, and t_y is the y-coordinate of the top marker. χ was calculated from the *y*- and *z*-coordinates for the top and bottom tether marks. ψ was calculated from the *x*- and *z*-coordinates for the left and right marks. The first frame was set to 0°, and the angle changes ($\Delta\eta$, $\Delta\chi$ and $\Delta\psi$) between each two successive frames were calculated. For example, l_x is the *x*-coordinate of the left marker from one frame, while l'_x is the *x*-coordinate of the left marker from the following frame. The formulas used were:

$$\Delta\eta = \tan^{-1}\left(\frac{(b'_x - b_x) - (t'_x - t_x)}{(t'_y - t_y) - (b'_y - b_y)}\right)$$

$$\Delta\chi = \tan^{-1}\left(\frac{(b'_y - b_y) - (t'_y - t_y)}{(t'_z - t_z) - (b'_z - b_z)}\right)$$

$$\Delta\psi = \tan^{-1}\left(\frac{(l'_x - l_x) - (r'_x - r_x)}{(r'_y - r_y) - (l'_y - l_y)}\right)$$

EMG spike times were extracted by performing amplitude-based event detections on each trace and marking the negative peak within each event (Figure 2.9). Depressor asymmetry (DA) was calculated by subtracting the firing time of the right M97 (RM97) from the firing time of the left M97 (LM97). Using this convention, a negative DA indicates that the LEMG fired before the REMG. Wing beat frequency (WBF) was calculated from the firing rate of left M97 (LM97).

Previously, McMillan et al. (2013) showed that η consistently changed approximately 40 ms after an EMG spike (implying that it took ~40 ms after an EMG spike for a change in rotation to occur). Thus, values for η, χ and ψ were measured 40 ms after the timing of EMG spikes. These values were exported for further analysis.

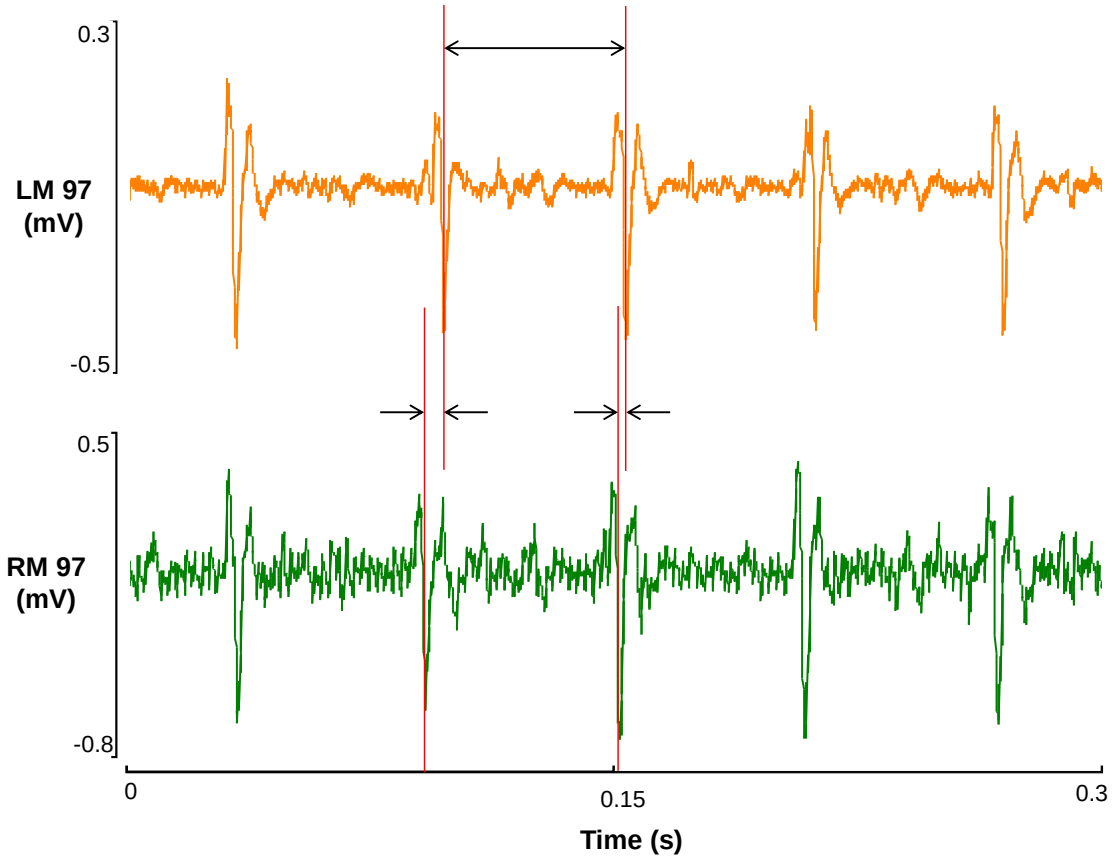

Figure 2.9 Sample electromyographic (EMG) recordings from one locust. The top channel (orange) shows the spikes from left M97 (LM97), while the bottom channel (green) shows the spikes from right M97 (RM97). The vertical red lines indicate that RM97 fired before LM97. The difference between LM97 and RM97 firing time was recorded as depressor asymmetry (DA). The duration between two successive LM97 firings were used to calculate LM97 firing rate, which is used to estimate the wing beat frequency.

2.6 STATISTICAL ANALYSIS

Statistical analysis was performed and plotted with SigmaPlot (SigmaPlot 12.5, Systat Software, San Jose, CA, USA). The timing and duration of behaviours were first tested for normality and equal variance. Parametric data were presented as the mean and standard deviation, while nonparametric data were presented as the median and the interquartile range. Differences in the timing and values of changes in select measured parameters (DA, η, χ, ψ and LM97 firing rate) were compared using a Student's t-test for parametric data and a Mann-Whitney rank sum test for nonparametric data. Related data was compared using a paired t-test (for parametric data) or Wilcoxon signed rank test (for nonparametric data). All tests were two-tailed and α was set at 0.05.

Pearson product-moment correlation (PPM) was used to test for relationships between DA and other variables. By convention, a range of operational definitions will be attributed to describe differences in the degree of correlation. PPM coefficient (r) values ranging from 0 to ±0.09 were considered to be not correlated, whereas values ranging from ±0.1 to ±0.29, ±0.3 to ±0.49, and ±0.5 to ±1 were considered as a small, medium or large correlation, respectively (Cohen, 1988).

CHAPTER 3. RESULTS

3.1 BODY ORIENTATION - SIMPLE BACKGROUND

3.1.1 GENERAL BEHAVIOURS

Against the simple background, each of 20 locusts was presented with two looms, comprised of a disc approaching from either the right or left at 45° azimuth. Thus, the entire dataset for a simple background consisted of a total of 40 approaches (trials). When first placed in the flight simulator, the locust would begin flapping its wings immediately after the wind supply was activated. Visual stimuli were presented once the locust maintained >1 minute of stable flight. Due to the size of the propeller (7 cm diameter), the wind supply was confined to a restricted volume of about 6,000 cm^3. Within this volume, the locusts continually conducted corrective steering manoeuvres, i.e., constantly adjusting the yaw (ψ) angles, to maintain upwind orientation of the head.

Initial observation of video files suggested that 8 of 40 trials showed a clear behavioural response, which occurred over multiple wing beats. In a previous study (McMillan et al., 2013), behavioural responses were categorized into turns, glides and stops. Movement towards or away from the stimulus during the approach was defined as a turn; momentary cessation of wing activity while the wings were elevated and held in a swept back dihedral position above the body was defined as a glide (Santer et al., 2005); cessation of flight and wings folded against the body was defined as a stop. Glides were not observed in the presence of simple background. Most of the trials with behavioural responses (N=7) were in the form of turns either away (N=4) or towards (N=3) the approaching object. One animal responded with a stop. These responses occurred in 8

different animals, i.e., no locusts responded to looming stimuli from both sides. In non-responding trials (N=32), locusts maintained the same orientation or constantly performed corrective steering during the approach of the visual stimuli. Given the difficulty in precisely assessing behaviours based on visual observations alone, I used an established, objective measure of the locust's position in 3-dimensional space to determine the time of behaviour (TOB). In each of the 40 trials, I calculated the double confinement ellipsoid (DCE) representing the locusts' flight trajectory from 2 to 1 s before TOC, and used the DCE to quantify the behavioural responses during object approach (Chan and Gabbiani, 2013) (Figure 3.1). In 33 out of 40 trials, the locust exited the DCE before the time of collision (TOC), including 14 animals that exited from approaches from both sides, and 5 that only responded to one side. The median of TOB was 0.87 s before TOC (interquartile range = 0.62 to 0.96 s before TOC).

3.1.2 STEERING

Translational degrees of freedom [TDOF (x, y, z coordinates of the locust)] and rotational degrees of freedom [RDOF, roll(η), pitch(χ) and yaw(ψ)] were calculated from the coordinates of four markers. These values describe the change of body orientation during flight. A right-handed coordinate system was used in the calculation. For TDOF: a positive x indicates a displacement to the right; a positive y indicates a displacement downwards; a positive z indicates a displacement forward. For RDOF: a positive η indicates a roll to the right; a positive χ indicates a pitch downwards; and a positive ψ indicates a yaw to the right.

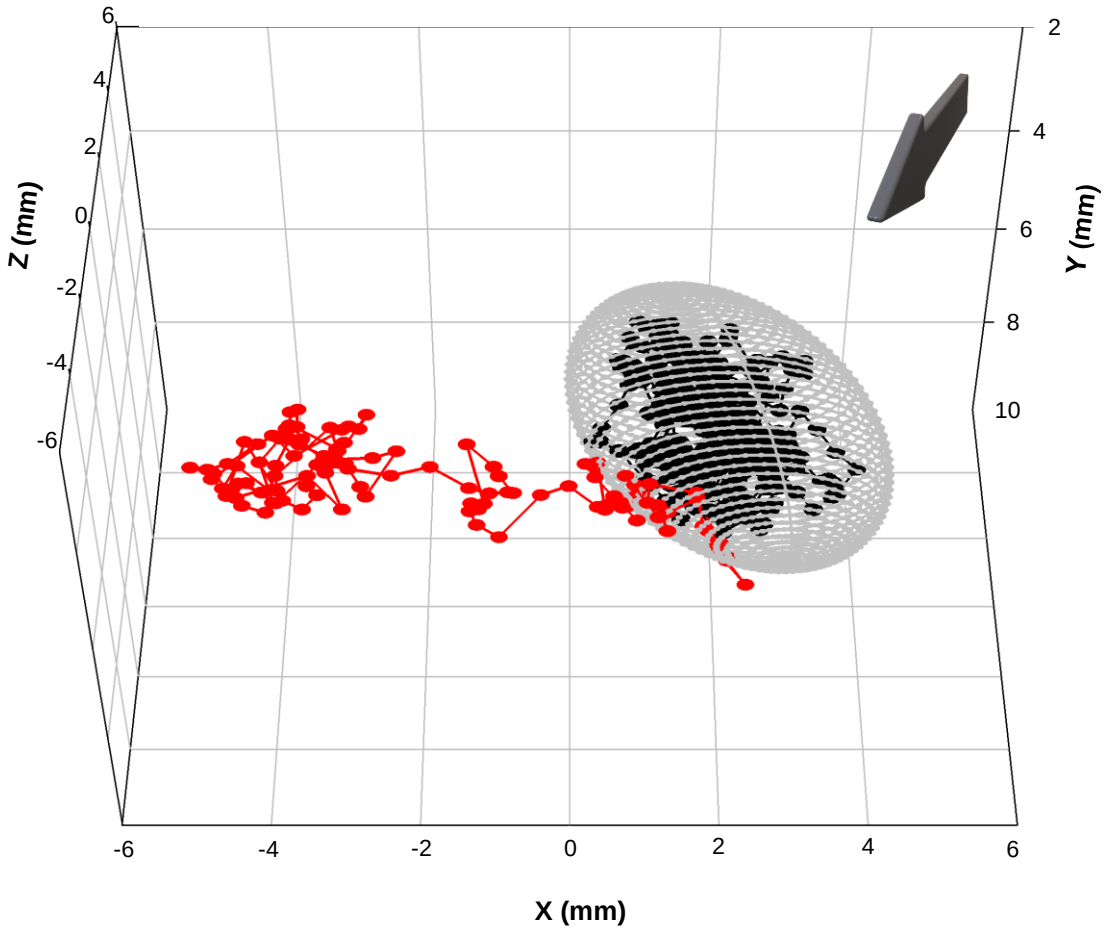

Figure 3.1 Three-dimensional flight trajectory tracking of one locust during collision avoidance behaviours. The arrow indicates the direction of the looming stimulus. The grey ellipsoid mesh represents the double confinement ellipsoid (DCE) that defines the pre-response epoch. The black dots represent the position of the locust during the pre-response epoch, while the red dots represent the position during the post-response epoch. Pre- and post-response epochs were defined by the time of behaviour (TOB) (Calculations shown in Figure 2.7).

Due to the corrective steering, TDOF and RDOF usually fluctuated within in an extent during the pre-response epoch. For *x*, the median extent was 4.08 mm (interquartile range = 2.98 to 5.50 mm); for *y*, the median extent was 7.29 mm (interquartile range = 7.15 to 7.44 mm); for *z*, the median extent was 3.45 mm (interquartile range = 2.73 to 4.31 mm). For η, the median extent was 20.3° (interquartile range = 16.3° to 24.3°); for χ, the median extent was 24.3° (interquartile range = 21.2° to 28.2°); for ψ, the mean extent was 54.9° (standard deviation = ± 20.2°). Figure 3.2 shows the changes of TDOF and RDOF, as well as DA and LM97 firing rate, of one trial in which the animal made a left turn in response to a looming stimulus approaching from right 45° azimuth. TOB and TOC were both labeled, indicating that the changes in TDOF and RDOF occurred simultaneously with behavioural responses. From TOB to TOC, the maximum *x* displacement was 7.28 mm to the left, whereas the *y* and *z* coordinates remained relatively steady, with a maximum y displacement of 1.72 mm downwards and a maximum z displacement of 3.81 mm forward. For RDOF, the maximum η change was 29.4° to the right; χ remained steady, with a maximum fluctuation of 30.1°; the maximum ψ change was 81.5° to the left. This fluctuation could potentially mask actual behavioural responses during collision avoidance attempts, and thus, I could not observe TOB-associated changes in RDOF in these trials.

3.2 MUSCLE ACTIVITY - SIMPLE BACKGROUND

3.2.1 LATENCY CHANGE DURING OBJECT LOOMING

During stable flight, the locust must generate symmetrical lift and thrust on each side of the body, which are produced by coordinated activity of approximately 40

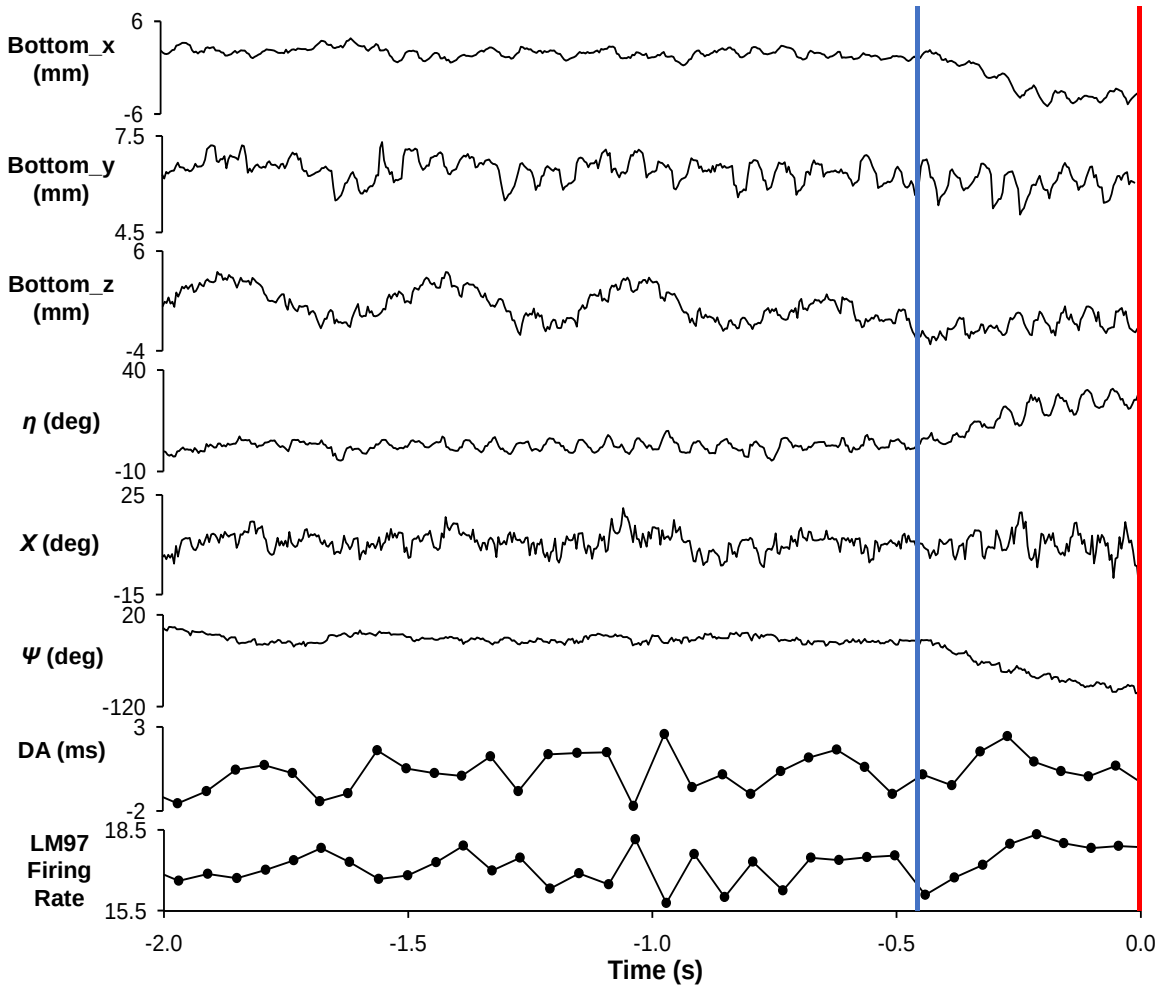

Figure 3.2 Concurrent EMG, kinematic and body orientation data of one trial in which the locust made a left turn. Data were aligned to the time of projected collision (TOC, red vertical line) of the looming stimulus. Bottom_x, Bottom_y and Bottom_z represent *x*-, *y*- and *z*-coordinates (translational degrees of freedom, TDOF) of the bottom marker of the tether, respectively. Roll(η), Pitch(χ) and Yaw(ψ) (rotational degrees of freedom, RDOF) were calculated as described in Figure 2.8. Depressor asymmetry (DA) was the firing time of right M97 subtracted from the firing time of the left L97. The LM97 firing rate was calculated from the firing time of the left forewing first basalar depressor muscle (M97). Since DA and LM97 firing rate were calculated from the firing time of M97, while the other measurements were calculated from video recordings, the sampling frequency of DA and LM97 were lower than the others. The blue vertical line represents the time of behaviour (TOB) (0.46 s before TOC).

muscles (Dawson et al., 1997). Changes in body orientation during flight result from asymmetrical steering torques that are generated by latencies in muscle firing times and these changes underlie collision avoidance (McMillan et al., 2013; Robertson and Reye, 1992; Robertson et al., 1996; Santer et al., 2005). Depressor asymmetry (DA) was calculated by subtracting the firing time of the right M97 (RM97) from the firing time of the left M97 (LM97). Using this convention, a negative DA indicates that the LM97 fired before the RM97.

The average and maximum difference of DA within each trial was calculated and pooled to evaluate the global trend. In the presence of a simple background, the global average of DA was 0.15 ms, with a standard deviation of ±2.4 ms. The global maximum difference of DA within each trial was 7.14ms, with a standard deviation of ±2.29 ms. There was no statistical difference in DA when looming stimuli approached from left or right 45° (independent t-test, $t = -0.08$, $P = 0.94$). A paired t-test comparing the latency of each pair of muscle spikes to the constant average latency across the entire trial showed that there was no statistical change in DA over time in 39 out of 40 trials (Paired t-test or Wilcoxon Signed Rank Test, $P > 0.05$). Only 1 out of 40 trials showed a statistical change in DA over time (Wilcoxon Signed Rank Test, $Z = -2.093$, $P = 0.037$). There was no significant difference in average DA whether the animal exited DCE or not (independent t-test, $t = 0.31$, $P = 0.76$) (Figure 3.3A). The DA from the last frame before TOB was compared with the average DA during the pre-response epoch to evaluate if there was a change in DA right before TOB. The results show that there was no significant change in DA before TOB (paired t-test, $t = 0.76$, $P = 0.45$) (Figure 3.4). In summary, there was no statistical difference in DA whether the looming stimuli

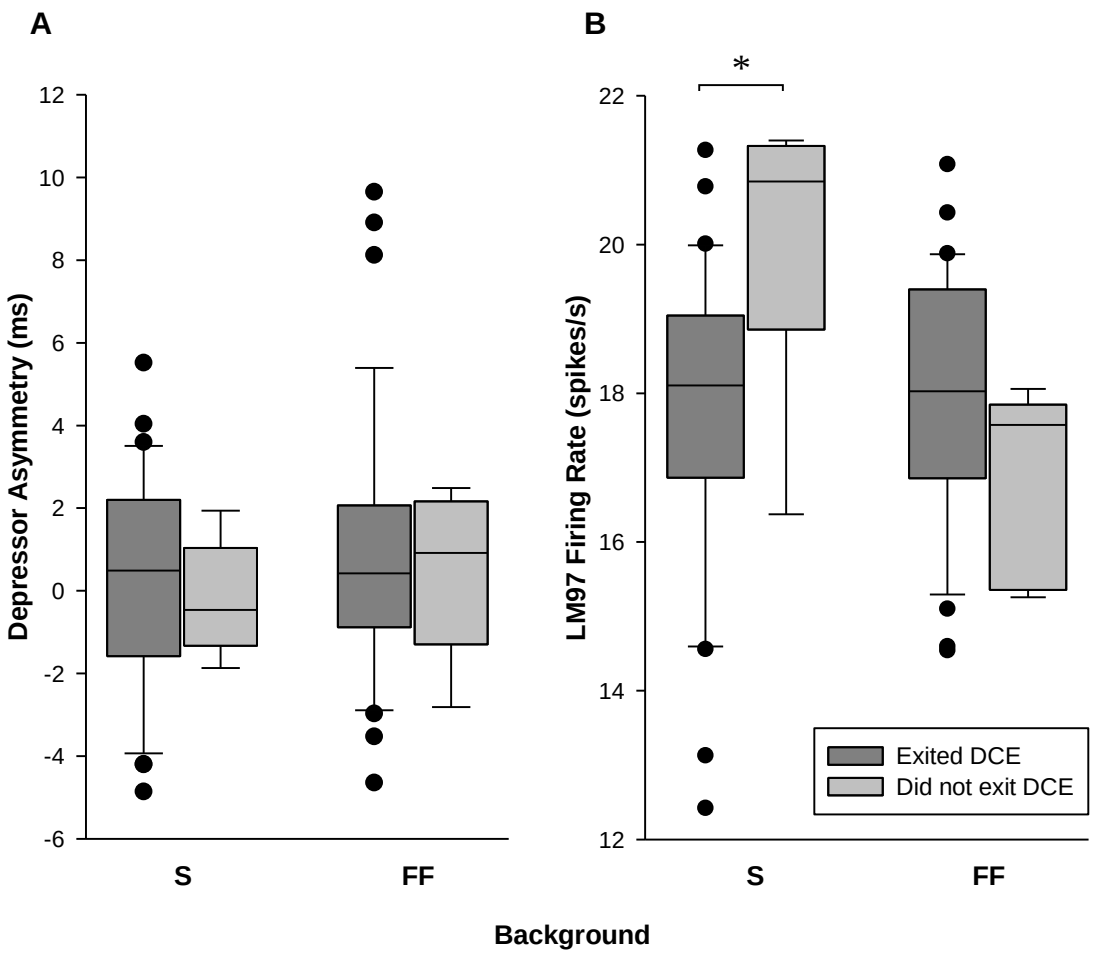

Figure 3.3 Comparison of depressor asymmetry (DA) and LM97 firing rate between animals that exited the double confinement ellipsoid (DCE) (Simple background, n = 33 approaches; Flow field background, n = 35 approaches) and those that did not (Simple background, n = 7 approaches; Flow field background, n = 5 approaches). **A.** Comparison of DA. **B.** Comparison of LM97 firing rate. The boxes represent the 25th and the 75th percentile. The error bars represent the 10th and the 90th percentile. The data points represent outliers. The * represents a statistical difference. In the presence of a simple (S) background, there was no significant difference in DA, while the animals that did not exit DCE had a significantly higher LM97 firing rate than those that exited (Mann-Whitney U Statistic= 43.000, P = 0.010). In the presence of a flow field (FF) background, there was no significant difference in both DA and LM97 firing rate whether the animal exited DCE or not. There was no statistical difference in DA and LM97 firing rate within different backgrounds.

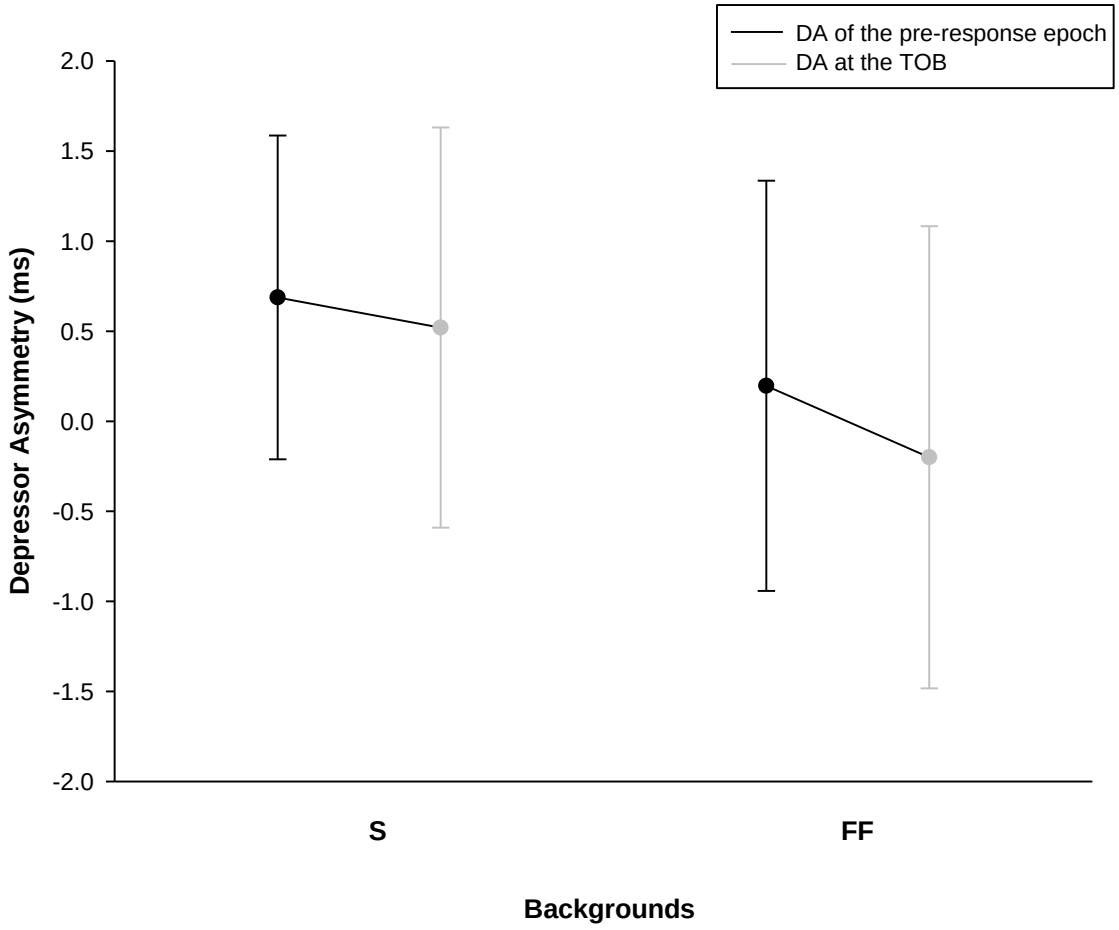

Figure 3.4 Comparison of the depressor asymmetry (DA) before and at the time of behaviour (TOB). The black points represent the median DA from the beginning of recording to the penultimate frame before TOB, while the grey points represent the DA at the last frame prior to TOB. The error bars represent the 95% confidence interval. As shown in the graph, in both backgrounds, there was no statistical difference between the DA of pre-response epoch and the DA at TOB. There was no statistical in DA within different backgrounds.

approached from left or right side. There was no statistical difference in DA whether the animal exited DCE or not. In 39 out of 40 trials, there was no statistical change in DA over time.

3.2.2 DEPRESSOR MUSCLE FREQUENCY

Since the firing of left M97 (LM97) has a one to one correspondence with wing beat, the firing rate of M97 equals the wingbeat frequency (WBF) of the flying locust. Despite the latency between left and right M97 firing, the overall firing rate is similar on both sides, and thus the firing rate of left M97 was used to study the WBF.

The average and maximum difference of LM97 firing rate within each trial was calculated and pooled to evaluate the global trend. In the presence of a simple background, LM97 firing rate remained relatively steady during each presentation. The global average LM97 firing rate was 18.2 spikes/s, with a standard deviation of ±2.1 spikes$\cdot s^{-1}$. The global median of the maximum difference within each trial was 2.8 spikes$\cdot s^{-1}$ (interquartile range =2.2 to 3.4 spikes$\cdot s^{-1}$). The LM97 firing rate was slightly higher when looming stimuli approached from left 45° (median = 18.90 spikes$\cdot s^{-1}$) than when they approached from the right 45° (median = 18.34 spikes$\cdot s^{-1}$) (Mann-Whitney U test, $U = 264338.5$, $P < 0.01$). The trials in which the animals exited DCE showed a lower LM97 firing rate than those that did not (Mann-Whitney U test, $U = 43.0$, $P = 0.01$) (Figure 3.3B).

3.3 CORRELATION BETWEEN MUSCLE TIMING AND FLIGHT BEHAVIOURS - SIMPLE BACKGROUND

3.3.1 OVERALL CORRELATION

Pearson product-moment (PPM) correlation coefficient (r) was calculated to evaluate the relationship between muscle timing latency and RDOF. The relationship between each RDOF [roll(η), pitch(χ), yaw(ψ)] and DA was first assessed. Since the RDOF were calculated from video recording, which have a higher sampling rate (250 frames$\cdot s^{-1}$) than the DA measurement, the behavioural data were down-sampled. McMillan et al. (2013) showed that RDOF consistently changed approximately 40 ms after an EMG spike. Therefore, I down-sampled the behavioural data such that the values from the frame closest to 40 ms after LM97 firing time was used in the correlation test. Among all 40 presentations against a simple background, 15 trials showed a significant correlation between DA and η, 2 trials showed a significant correlation between DA and χ, and 20 trials showed a significant correlation between DA and ψ. When comparing the trials with looming stimuli coming from different directions, more animals showed a significant correlation when the stimuli came from the right side (Figure 3.5) (details in Table 3.1).

PPM coefficient (r) values ranging from 0 to ±0.09 were considered to be not correlated, whereas values ranging from ±0.1 to ±0.29, ±0.3 to ±0.49, and ±0.5 to ±1 were considered as a small, medium or large correlations, respectively (Cohen, 1988). When a significant correlation existed, the absolute values of r between DA and RDOF were all larger than 0.3, indicating medium or higher correlations. However, the positive or negative signs were not consistent. For η, 12 of 15 trials showed positive correlation,

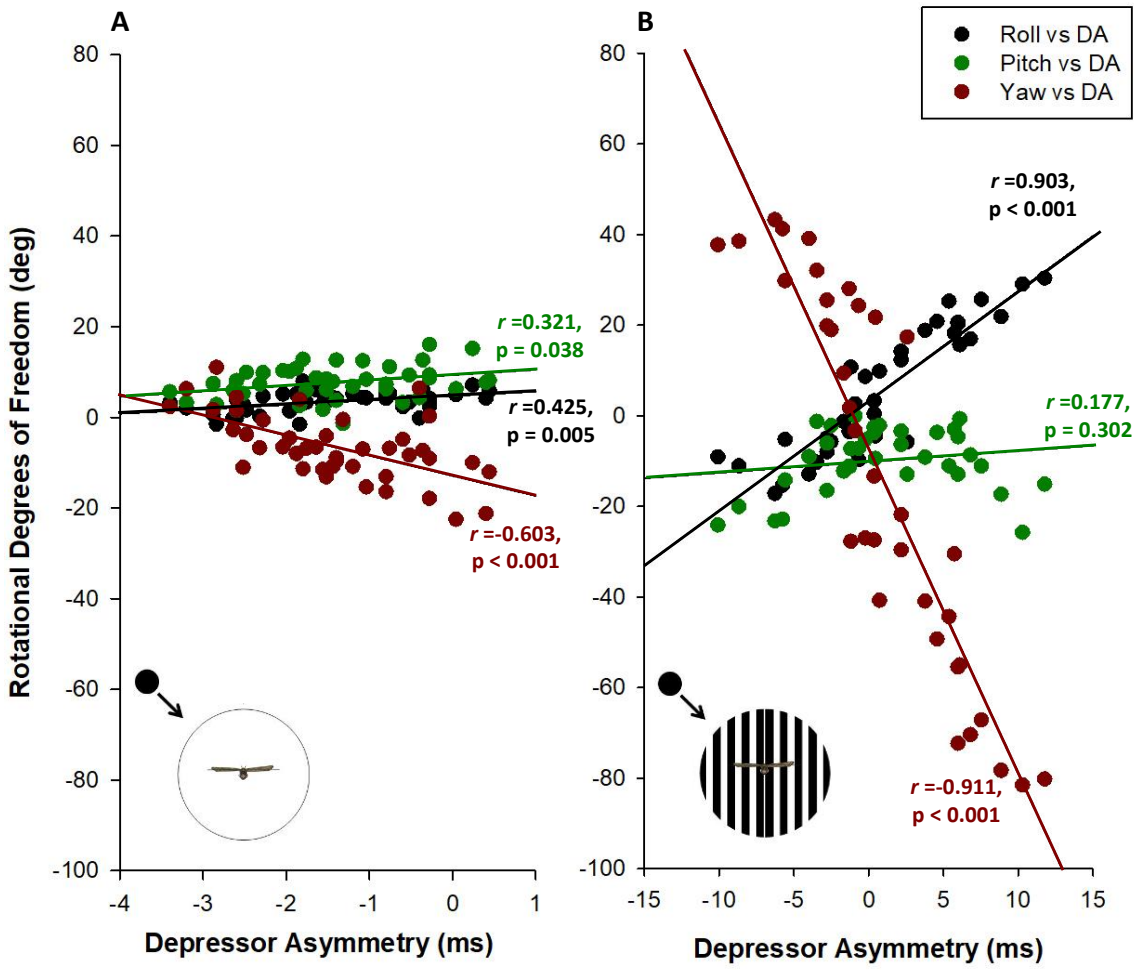

Figure 3.5 Scatter plot demonstrating the Pearson product-moment correlation (PPM) between rotational degrees of freedom (RDOF) and depressor asymmetry (DA) of a locust responding to a looming stimulus approaching against different backgrounds. **A.** Simple background. **B.** Flow field background. Black dots represent roll (η), green dots represent pitch (χ), and red dots represent yaw (ψ). Black lines represent the regression line between each RDOF and DA. As shown in the graph, against a simple background, the correlations between each RDOF and DA in this trial were all significant (Pearson product-moment correlation, $P < 0.05$). However, in a flow field background, the correlation between pitch and DA was not significant, while the correlation between the other RDOFs (roll and yaw) and DA were significant (Pearson product-moment correlation, $P < 0.05$). Overall, I found significant correlation between RDOFs and DA in more trials with a simple background compared to those with a flow field background. Detailed counting shown in Table 3.1.

			Positive Correlation	Negative Correlation	No Correlation	Range of $\|r\|$	
RDOF	S	η vs DA	12	3	25	0.33 – 0.66	*
		χ vs DA	1	1	38	0.32 – 0.36	
		ψ vs DA	5	15	20	0.31 – 0.65	
	FF	η vs DA	4	0	36	0.35 – 0.90	*
		χ vs DA	3	1	36	0.35 – 0.41	
		ψ vs DA	6	0	34	0.35 – 0.91	
ΔRDOF	S	$\Delta\eta$ vs DA	2	2	36	0.34 – 0.50	
		$\Delta\chi$ vs DA	0	2	38	0.34 – 0.37	
		$\Delta\psi$ vs DA	2	3	35	0.32 – 0.34	
	FF	$\Delta\eta$ vs DA	2	2	36	0.35 – 0.52	
		$\Delta\chi$ vs DA	0	3	37	0.37 – 0.52	
		$\Delta\psi$ vs DA	2	1	37	0.37 – 0.43	

Table 3.1. Summary of overall correlations between rotational degrees of freedom (RDOF) and depressor asymmetry (DA). RDOF represents the values of η, χ and ψ, while ΔRDOF represents the change in η, χ and ψ from the previous frame. S represents simple background, while FF represents flow field background. The Pearson Product Correlation between each RDOF and DA was calculated for each trial. The total number of trials for each row was 40 (20 animals, 2 looms each). As shown in the table, more trials showed significant correlations between DA and RDOF during presentation against a simple background than the flow field background. The last column shows the range of $|r|$ in the trials with significant correlation.

while 3 of 15 showed negative correlation. For χ, 1 of 2 showed positive correlation, while 1 of 2 showed negative correlation. For ψ, 5 of 20 showed positive correlation, while 15 of 20 showed negative correlation. This result showed that the change in η and ψ could be predicted by DA in most cases. However, in some trials (3 out of 15 for η and 5 out of 20 for ψ) the correlation was reversed.

Since whole-body movement was dynamically adjusted by asymmetric wing movements, the relationship between DA and RDOF change between two successive frames [ΔRDOF ($\Delta\eta$, $\Delta\chi$, $\Delta\psi$)] could potentially provide additional information. However, among 40 presentations, 4 trials showed a significant correlation between DA and $\Delta\eta$, 2 trials showed a significant correlation between DA and $\Delta\chi$, and 5 trials showed a significant correlation between DA and $\Delta\psi$. All the correlations were medium or higher ($|r| > 0.3$).

In summary, η and ψ showed significant correlation with DA in more trials, compared to χ. The positive or negative signs of the correlations were not consistent. Compared to η, χ and ψ, $\Delta\eta$, $\Delta\chi$ and $\Delta\psi$ showed significant correlation with DA in fewer trials.

3.3.2 CORRELATION CHANGES OVER TIME

To assess how the correlation changed over time, all 40 trials were time-aligned to TOC, and the entire recording time (2 seconds) was divided into 40 ms bins. Data that fell into the same bin were pooled to evaluate the PPM correlation across all trials. The

PPM correlation coefficient (r) from each bin reflected the trend of correlation coefficients.

For correlation between DA and RDOF in all 50 bins, only 1 bin showed a significant correlation between DA and η, 8 bins showed a significant correlation between DA and χ, and 1 bin showed a significant correlation between DA and ψ. When a significant correlation existed, all these correlations were medium or higher ($|r|$ ranging from 0.365 to 0.532) (Figure 3.6A). For η, the bin that showed a significant correlation occurred in the interquartile range of TOB, and it had the lowest r value (-0.396); for χ, 4 correlated bins occurred during the pre-turn epoch, and 4 occurred after the interquartile range of TOB; for ψ, the bin that showed a significant correlation occurred after the interquartile range of TOB. The timing of these bins indicates that the correlation between DA and RDOF was not a strong predictor of the animal's behaviour.

For correlation between DA and ΔRDOF in all 50 bins, 4 bins showed a significant correlation between DA and $\Delta\eta$, 3 bins showed a significant correlation between DA and $\Delta\chi$, and 1 bin showed a significant correlation between DA and $\Delta\psi$. All these correlations were medium ($|r|$ ranging from 0.383 to 0.454) (Figure 3.7). For $\Delta\eta$, 3 out of 4 bins occurred before median TOB, and 1 occurred in the interquartile range of TOB; for $\Delta\chi$, 1 out of 3 bins occurred during pre-response epoch, 1 bin occurred in the interquartile range of TOB, and the other occurred near TOC; for $\Delta\psi$, this bin occurred in the interquartile range of TOB, and it has the highest r value (0.396). This bin also occurred at the same time as 1 of the bins that showed a significant correlation between DA and $\Delta\eta$, which is 0.03 s after median TOB (0.87 s before TOC). Even though it

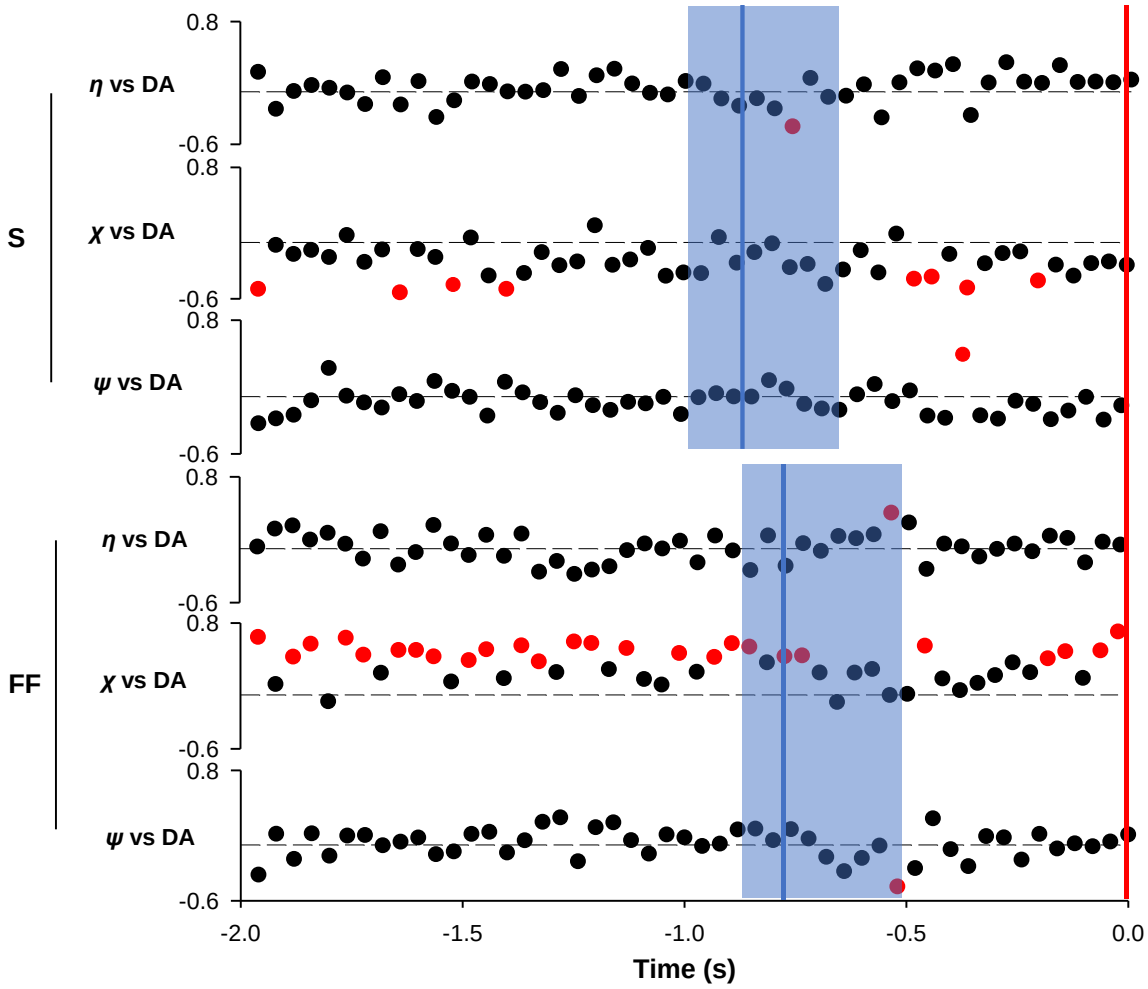

Figure 3.6 Changes in correlation between the rotational degrees of freedom [RDOF (η, χ and ψ)] and the depressor asymmetry (DA) over time. RDOF was down-sampled at 40 ms after a left M97 spike (see methods for details). The red vertical line represents the time of collision (TOC), while the blue lines represent the median time of behaviour (TOB). The blue shadow represents the interquartile range of TOB. Each dot represents the Pearson product moment correlation coefficient (r) between an RDOF (η, χ and ψ) and DA for all 40 trials in a 40 ms time bin. The dashed line represents 0. A black dot indicates that there was no significant correlation in that bin, whereas a red dot indicates that there was a significant correlation. S represents the simple background, while FF represents the flow field background. In the simple background, no TOB-related changes in the correlation was observed. In the flow field background, the correlation between χ and DA became insignificant 0.06 s after median TOB. Even though it occurred after median TOB, it is possible that in individual trials, the time occurred before TOB.

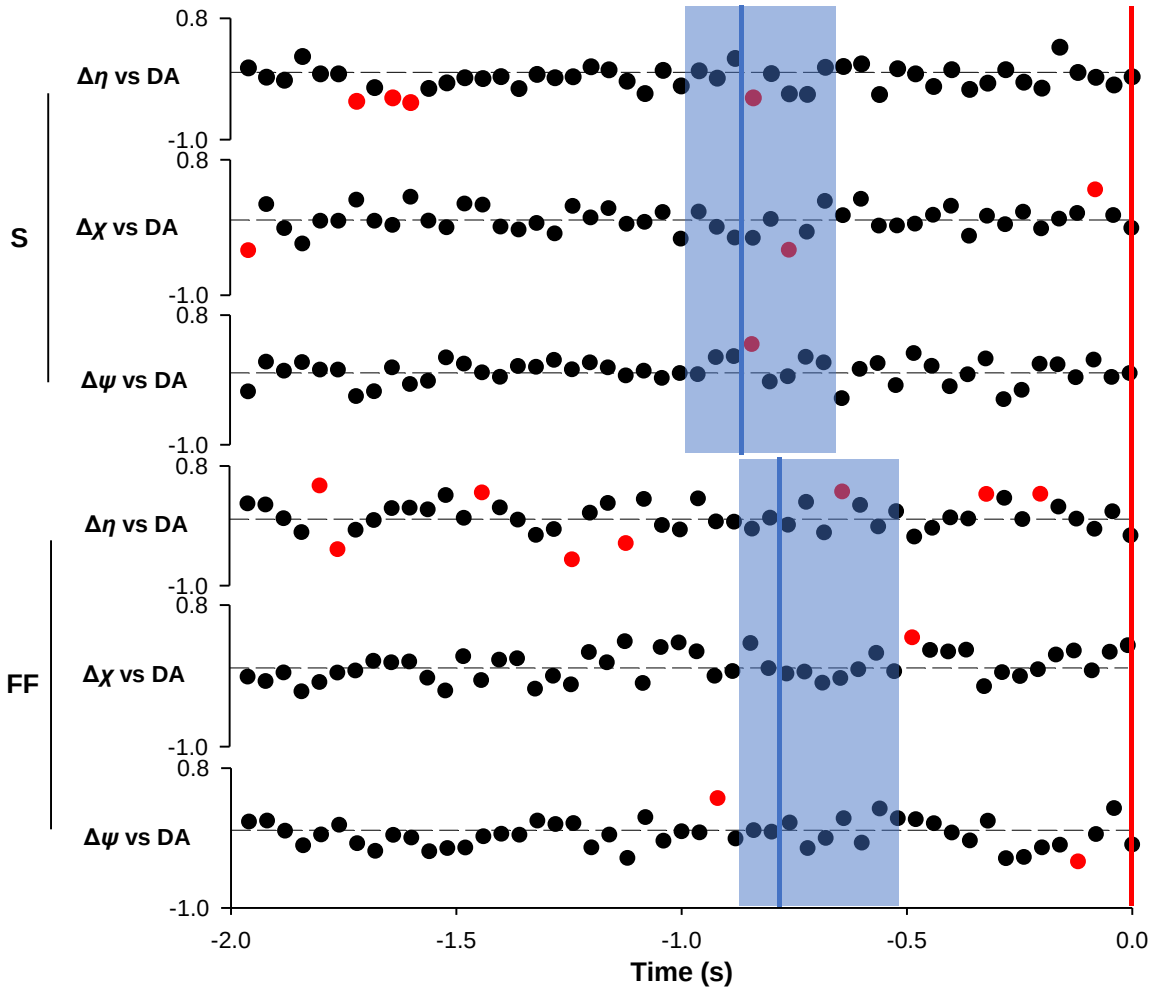

Figure 3.7 Changes in correlation between ΔRDOF ($\Delta\eta$, $\Delta\chi$ and $\Delta\psi$) and the depressor asymmetry (DA) over time. ΔRDOF was the RDOF change between two successive frames. The red vertical line represents the time of collision (TOC), while the blue lines represent the median time of behaviour (TOB). The blue shadow represents the interquartile range of TOB. Each dot represents the Pearson product moment correlation coefficient (r) between an ΔRDOF ($\Delta\eta$, $\Delta\chi$ and $\Delta\psi$) and DA for all 40 trials in a 40 ms time bin. The dashed line represents 0. A black dot indicates that there was no significant correlation in that bin, whereas a red dot indicates that there was a significant correlation. S represents the simple background, while FF represents the flow field background. In the simple background, the correlation between two ΔRDOFs ($\Delta\eta$ and $\Delta\psi$) and DA became significant 0.03s after median TOB. Even though it occurred after median TOB, it is possible that in individual trials, the time occurred before TOB. In the flow field background, the correlation between $\Delta\psi$ and DA first became significant 0.14s before median TOB.

occurred after median TOB, it is still within the interquartile range of TOB, suggesting a potential correlation with the behaviour time.

Overall, the correlation between DA and RDOF was not well related with the timing of TOB, while the correlation between DA and ΔRDOF ($\Delta\eta$ and $\Delta\psi$) might predict the timing of TOB. Near median TOB (0.03 s), these correlations became significant.

3.4 EFFECT OF BACKGROUND COMPLEXITY

3.4.1 BEHAVIOURS

The same 20 animals were also presented with looming stimuli approaching from right or left 45 degrees azimuth within a flow field (FF) background for a total of 40 presentations (trials). The order of the 4 visual stimuli (left or right, simple or flow field background) were randomized for each animal. In all 40 trials with flow field background, initial observation of video files suggested behavioural responses in fewer trials (5 out of 40) compared to those in the presence of a simple background (8 out of 40), with responses occurring over multiple wing beats. These responses include 4 turns away from looming and 1 glide. These responses occurred in 5 different animals, i.e. no locusts responded to looming stimuli from both sides. Other animals maintained the same orientation or constantly performed corrective steering during the approach of visual stimuli.

3D motion tracking showed that in 35 out of 40 trials, the animal exited DCE before TOC, including 16 animals that exited from approaches from both sides, and 3 that

only responded to one side. The median TOB was 0.78 s before TOC (interquartile range = 0.52 to 0.88 s before TOC). Compared to data from simple background trials (median = 0.87 s before TOC), TOB occurred slightly later in the presence of a flow field. However, the difference between the two backgrounds was not statistically significant (Mann-Whitney U test, $U = 459.0$, $P = 0.15$).

Similar to the trials within simple background, TDOF and RDOF also fluctuated during the pre-response epoch. For x, the median extent was 3.60 mm (interquartile range = 2.72 to 4.97 mm); for y, the median extent was 7.39 mm (interquartile range = 7.21 to 7.60 mm); for z, the median extent was 3.79 (interquartile range = 3.08 to 4.46 mm). For η, the median extent was 19.2° (interquartile range = 16.2° to 22.6°); for χ, the median extent was 24.1° (interquartile range = 22.6° to 26.5°); for ψ, the median extent was 49.5° (interquartile range = 38.0° to 64.4°). This fluctuation due to corrective steering could potentially mask the behavioural responses during collision avoidance attempts.

3.4.2 MUSCLE ACTIVITY AND DEPRESSOR MUSCLE FREQUENCY

In the presence of flow field background, the median of average DA was 0.4ms (interquartile range = -0.6 ms to 1.9 ms). Within each presentation, DA remained relatively steady. The median of the maximum difference of DA within each trial was 7.6 ms (interquartile range = 4.2 ms to 9.1ms). There was no statistical difference in DA when looming stimuli approached from left or right 45° (Mann-Whitney Rank Sum Test, $U = 73.0$, $P = 0.082$). There was no statistical difference in average DA whether the animal exited DCE or not (Mann-Whitney U test, $U = 77.0$, $P = 0.683$) (Figure 3.3A). A paired t-test comparing the latency of each pair of muscle spikes to the constant average latency across the entire trial showed that there was no statistical change in DA over time

in all 40 trials (paired t-test, $P = 1.00$, or Wilcoxon Signed Rank Test, $P > 0.05$). There was no significant change in DA before TOB (Mann-Whitney U test, $U = 596.0$, $P = 0.851$) (Figure 3.4). In summary, similar to the trials within the simple background, there was no difference DA whether the looming stimuli approached from left or right side, or if the animal exited DCE. All 40 trials showed no statistical change in DA over time.

In the presence of flow field background, the LM97 firing rate (wing beat frequency) remained relatively steady during each presentation. The global average LM97 firing rate was 17.8 spikes$\cdot s^{-1}$, with a standard deviation of ± 0.62 spikes$\cdot s^{-1}$. The median of the maximum difference of LM97 firing rate was 3.2 spikes$\cdot s^{-1}$(interquartile range = 2.4 to 3.8 spikes$\cdot s^{-1}$). There was no significant difference in LM97 firing rate whether the stimuli approached from left or right (Mann-Whitney U test, $U = 269534.000$, $P = 0.487$). There was no significant difference in LM97 firing rate whether the animals exited DCE or not (independent t test, $t = 4.15$, $P = 0.155$) (Figure 3.3.B).

In summary, compared to simple background, the average DA was slightly higher in flow field background, and the fluctuation within each trial was larger. LM97 firing rate was slightly lower. However, none of these differences were statistically significant.

3.4.3 CORRELATION

3.4.3.1 OVERALL CORRELATION

The relationship between RDOF (η, χ, ψ) and DA was evaluated. Among all 40 trials within flow field background, 4 trials showed a significant correlation between DA and η, 4 trials showed a significant correlation between DA and χ, and 6 trials showed a

significant correlation between DA and ψ. When comparing the trials with looming stimuli approaching from different directions, more animals showed a significant correlation when the stimuli came from the right side (Figure 3.5) (details in Table 3.1).

The absolute values of PPM correlation coefficient (r) between DA and RDOF were larger than 0.3, indicating medium or large correlation, and the positive or negative signs were consistent except for χ. For η, all 4 trials with significant correlation were positive. For χ, 2 trials with significant correlation were positive while 2 were negative. For ψ, all 6 trials with significant correlation were positive. The trend in η was the same as shown in simple background, however the trend in ψ was opposite. In simple background, most of the trials with significant correlation between DA and ψ showed a negative correlation.

The relationship between DA and ΔRDOF ($\Delta\eta$, $\Delta\chi$, $\Delta\psi$) was then assessed. Among 40 presentations, 4 trials showed a significant correlation between DA and $\Delta\eta$, 3 trials showed a significant correlation between DA and $\Delta\chi$, and 3 trials showed a significant correlation between DA and $\Delta\psi$. All the correlations were medium or higher ($|r| > 0.3$). For $\Delta\eta$, 2 out of 4 trials showed a positive correlation while 2 showed a negative correlation. For $\Delta\chi$, all 3 trials showed a negative correlation. For $\Delta\psi$, 2 trials showed a positive correlation while 1 showed a negative correlation.

Compared to simple background, fewer trials showed significant correlation between DA and RDOF in flow field background (Fisher's exact test, $P < 0.05$), while the number of trials that showed significant correlation between DA and ΔRDOF were similarly low (Fisher's exact test, $P > 0.05$). The positive or negative signs were similar for η and $\Delta\eta$ in different backgrounds. However, the pattern was opposite for ψ and $\Delta\psi$.

3.4.3.2 CORRELATION CHANGES OVER TIME

In FF background, for correlation between RDOF and DA, only 1 out of 50 bins showed a significant correlation between DA and η, 26 bins showed a significant correlation between DA and χ, and 1 bin showed a significant correlation between DA and ψ. All these correlations were medium or higher ($|r|$ ranging from 0.37 to 0.703) (Figure 3.6). The timing of these bins for η and ψ were 0.26s after median TOB (still within the interquartile range of TOB), and they, respectively, have the highest or the lowest r value (η :0.399, ψ: -0.448). For χ, the correlation was mostly significant (20 out of 31 bins) until 0.06s before median TOB, and r reached its lowest point (-0.08) during the interquartile range of TOB, suggesting a decreased correlation near the time of a behavioural response.

For correlation between ΔRDOF and DA, 8 out of 50 bins showed a significant correlation between DA and $\Delta\eta$, 1 bin showed a significant correlation between DA and $\Delta\chi$, and 2 bins showed a significant correlation between DA and $\Delta\psi$. All these correlations were medium or higher ($|r|$ ranging from 0.364 to 0.609) (Figure 3.7). For $\Delta\eta$, 5 out of 8 bins occurred in pre-response epoch, 1 occurred in the interquartile range of TOB, and 2 occurred after the interquartile range of TOB. For $\Delta\chi$, the only bin occurred 0.3s after median TOB. For $\Delta\psi$, 1 bin occurred before median TOB, while the other occurred after median TOB. The 1st bin occurred 0.14s before median TOB, with the highest r value (0.411), suggesting an increase in correlation before the behavioural response.

Compared to S background, the correlation between DA and χ in FF background was higher, while the correlations between DA and other RDOF were lower. The

correlation between DA and ΔRDOF were similarly low in both S and FF background. The timing of the significant correlations in FF background showed a different pattern from that shown in S background: the correlation between DA and χ became lowest during the interquartile range of TOB, which was not shown in the S background; the correlation between DA and $\Delta\eta$ also became significant in the interquartile range of TOB, while the correlation between DA and other ΔRDOF did not.

CHAPTER 4. DISCUSSION

4.1 SUMMARY OF RESULTS

This is the first study to investigate concurrent muscle activity and behavioural responses of a flying locust exposed to complex visual environments. Previous studies investigating locust collision detection revealed that the LGMD/DCMD pathway encodes the looming stimuli via changes in firing frequency (Gabbiani et al., 1999; Gray et al., 2001; Hatsopoulos et al., 1995; Judge and Rind, 1997; Rind and Simmons, 1992; Santer, 2006; Schlotterer, 1977), and a bursting firing pattern (Dick et al., 2017; McMillan and Gray, 2015). More recently, flight muscle activity and body orientation have been recorded in loosely-tethered locusts exposed to simplified visual stimuli (Chan and Gabbiani, 2013; McMillan et al., 2013). However, real-world visual environments are typically complicated, containing many objects and patterns of optic flow, which modulate DCMD responses (Guest and Gray, 2006; Silva et al., 2015). Therefore, to better understand mechanisms underlying collision avoidance behaviour of the locust, it was important to investigate how background complexity may affect loosely-tethered flying locusts during presentation of an approaching object. Utilization of this tractable system will inform general fundamental concepts of the neural control of adaptive behaviour.

In the presence of a simple background, locusts exited the double confinement ellipsoid (DCE) that defines the pre-response epoch in 33 out of 40 trials, and the median time of behaviour (TOB) was 0.87 s before time of collision (TOC). No TOB-associated changes in translational degrees of freedom (TDOF) or rotational degrees of freedom

(RDOF) were observed. Depressor asymmetry (DA) and the LM97 firing rate did not change significantly during an approach. Compared to pitch (χ), roll (η) and yaw (ψ) showed a significant correlation with DA in more trials. During the interquartile range of TOB, the correlations between η, as well as all three ΔRDOFs ($\Delta\eta$, $\Delta\chi$ and $\Delta\psi$), and DA became significant (Pearson product-moment correlation, $P < 0.05$).

In the presence of a flow field background, the animal exited DCE in 35 out of 40 trials, and the median TOB was 0.78 s before TOC. Similar to approaches against a simple background, no TOB-associated changes in TDOF and RDOF were observed. DA and LM97 firing rate did not show significant changes during any trials. Fewer trials showed significant correlation between DA and RDOF in flow field background compared to simple background. The correlation between DA and χ was mostly significant (20 out of 31 bins) and became insignificant 0.06 s before median TOB. The correlation between DA and two RDOF (η and ψ) as well as $\Delta\eta$ became significant during the interquartile range of TOB.

In summary, the general behavioural responses of the locusts were similar in the presence of either background. There was no significant difference in TOB between background types. For a flow field background, I found significant correlations between DA of M97 and RDOF in fewer trials compared to a simple background. For a simple background, the correlations between DA and certain RDOF/ΔRDOF (η, $\Delta\eta$, $\Delta\chi$, and $\Delta\psi$) became significant during the interquartile range of TOB. In a flow field background, the correlation between DA and certain RDOF/ΔRDOF (η, ψ, $\Delta\eta$) became significant during the interquartile range of TOB, while the correlation between DA and χ became insignificant and reached its lowest value during the interquartile range of TOB.

4.2 TECHNICAL AND EXPERIMENTAL CONSIDERATIONS

In order to initiate and maintain the locust flight in the flight simulator, the locust tether, wind supply and recording systems were re-designed to enable the locust to fly while complex visual stimuli could be projected. Nevertheless, there were caveats with the experimental setup. The addition of the tether and electrodes could have affected the flight behaviour of the locust. The total weight of the tether was ~0.3 g, which is 15% of the average locust's body weight (~2 g). The electrodes (weight = ~0.08 g) hanging from the bottom could also drag the locust down. However, a similar setup has been used previously by McMillan et al. (2013), and they described robust flight and steering with similar electrode and tether placement.

The propeller provided a wind supply to initiate and maintain the locusts' flight. It was mounted in front of the locust, and thus could block the view of stimuli. However, the propeller was colourless, and we could not retrieve a clear image of the blades from the camera recordings, the frame of which (250Hz) was over 3.5 times the average flicker fusion frequency of the locust's eye (66.3 Hz) (Miall, 1978). Therefore, the rotating propeller likely did not interfere spatially or temporally with the locust's field of view.

Due to the limited volume of the wind supply (a cylinder-shaped area with a volume of ~6,000 cm^3), the free length of the fishing line was restricted by a capillary tube to restrain the locust within this volume. McMillan et al. (2013) recorded from flying locusts in the wind tunnel, which could offer consistent wind flow in a very large area, thus evoking more stable flight. If the size of the propeller was increased, and a suction pump was mounted behind the animal, the volume of the area with wind supply would increase, and the wind speed could be more uniform. This would result in more

stable flight during the pre-response epoch, and reduce the fluctuation of TDOF and RDOF, which could potentially lead to more accurate assessment of behavioural responses. However, the restricted flight freedom was useful in aligning TOC. If the tether was longer, the locust would be able to maneuver in a larger range, and thus the expected TOC would vary considerably between individual trials. Additionally, a larger propeller and suction pump would create more noise, which might affect the locust's response as well. The setup used in the experiment was a necessary compromise that enabled video and EMG recordings with the locust free to manoeuvre in 3D space, while further testing with different setups would be necessary to fully optimize stable flight generation.

In the flight simulator, despite the visual flow projected on the dome screen, the rear view of the locust was stationary and thus could confound the sense of motion. However, the setup was consistent with previous studies with rigidly tethered locusts (Parkinson et al., 2017; Silva et al., 2015), and it did evoke flight and steering behaviours (Manchester *et al.*, unpublished data). Previous studies have found differential ommatidial density between different parts of the locust eye, with a maximum in the frontal region (Horridge, 1978; Krapp and Gabbiani, 2005). However, DCMD responses to looming were invariant across 135° of azimuth (Gabbiani et al., 2001). Thus, even though the flow field background was only applied to the frontal visual field, it would be sufficient to investigate the effect of different visual backgrounds.

In the current setup, lighting was provided by an infrared lamp. However, at the current location, the reflection of infrared light on the dome occasionally overlapped with the locust, which made the locust's wing movement difficult to measure from the video

recordings. Previous studies have investigated the change of wing asymmetry during collision avoidance behaviour of loosely-tethered locusts (McMillan et al., 2013). If the placement of the lamp was adjusted, the wing asymmetry would be measurable, which could provide another dimension of behavioural information. However, this did not affect the measurements made from the tether.

4.3 INTERPRETATION OF RESULTS

In the presence of a simple background, the animals that exited DCE showed a lower LM97 firing rate. This is likely because the animals with a higher LM97 firing rate maneuvered in a larger space during the pre-response epoch, and thus the DCE that defined the pre-response epoch was larger. As a result, even if the animal did perform a collision avoidance behaviour, its flight trajectory was within the same area, and thus it did not exit DCE.

When calculating the maximum difference of DA within each trial, the greatest value was 21.8ms (median = 7.6 ms, range = 2.9 ms to 21.8ms). This was due to the animal changing orientation during the pre-response epoch. DA was calculated by subtracting the firing time of the right M97 (RM97) from the firing time of the left M97 (LM97). Ideally, locusts fly straight upwind (Chapman, 1959; Kennedy, 1951; Waloff, 1972). In this case, the locust depresses both wings simultaneously to generate equal bilateral lift and thrust, and thus DA should be close to 0 ms. However, due to the corrective steering, the animals would fly at a certain angel away from 0° azimuth. When the animal was flying towards the left, DA would be positive and when flying towards the right, DA would be negative. If the animal changed orientation during a trial, the

maximum difference within this trial would be higher than anticipated. This was not observed in the wind tunnel (Chan and Gabbiani, 2013; McMillan et al., 2013).

In the presence of a simple background, the LM97 firing rate was higher when the looming stimulus approached from left 45° (median = 18.90 spikes/s) than when it approached from the right 45° (median = 18.34 spikes/s) (Mann-Whitney U test, U = 264338.500, P = 0.001). Recently, Ong et al. (2017) reported that honeybees (*Apis mellifera*) may have a preference of side when deciding to fly through one of two apertures, suggesting the existence of handedness in individual animals (Ong et al., 2017). The difference in LM97 firing rate might suggest an effect of the orientation of looming stimuli on the wing beat frequency, indicating potential effect of handedness. However, the effect size was very low. Even though the difference was statistically significant, it may not be biologically relevant, and thus further experiments are required to rigorously test whether locusts have a preferred direction of motion.

4.4 COMPARISON WITH PREVIOUS FINDINGS

Previously, flight muscle activity, wing kinematics and aerodynamic forces of locusts have been recorded during collision avoidance behaviour and measured from rigidly-tethered locusts flying in open-loop conditions (Gray et al., 2001; Hedwig and Becher, 1998; Ribak et al., 2012; Robertson and Johnson, 1993; Robertson and Reye, 1992; Santer, 2006; Santer et al., 2005; Simmons et al., 2010). Using minimally a restrained preparation, Chan and Gabbiani (2013) measured several behavioural parameters, including wing kinematics and body rotations, which had not been described in rigidly tethered preparations. Using a combination of EMG recordings and video-based

motion analysis on loosely-tethered flying locusts, McMillan et al. (2013) described the relationships between forewing depressor muscle activity, wing kinematics and 3-dimensional body orientation related to responses to lateral looming visual stimuli. Using a similar setup, Manchester *et al.* (unpublished) investigated the timing and synchrony of multiple flight muscles, correlating them with wing kinematics and whole-body motion. Compared to wind tunnel experiments, locusts in the flight simulator showed higher variation in behavioural responses and M97 activity. Fewer trials showed significant correlation between DA and RDOFs. However, changes in the correlation could still be related to TOB.

The flow field background, which mimics the optic flow produced during locust flight, was applied to investigate the effect of visual background. In rigidly-tethered locusts, the presence of flow field background caused reduced firing rates, delayed peaks, shorter rise phases, and longer fall phases in DCMD responses. Spike numbers were also reduced in the flow field background (Silva et al., 2015). However, my data suggests that there was no significant difference in TOB within different backgrounds, suggesting varying processing time between DCMD response and depressor muscle activities. Numerous interneurons located in the thoracic ganglia project to the motorneurons that control the wing movements. Further investigation into this modulation network is required to understand where the difference came from.

4.5 CONCLUSIONS

In summary, in the presence of a simple background, most animals exited the area representing the pre-response epoch before TOC, indicating collision avoidance

responses. However, the timing of TOB varied among different animals, and no changes in DA and LM97 firing rate were observed before TOB. η and ψ showed significant correlation with DA in more trials, compared to χ. The time when the correlation between RDOF/ΔRDOF (η, $\Delta\eta$, $\Delta\chi$, and $\Delta\psi$) and DA became significant occurred during the interquartile range of TOB.

In the presence of a flow field background, the responses of the animals were similar to those in a simple background. DA and LM97 firing rate showed no difference with those in simple background. Fewer trials showed significant correlation between M97 DA and RDOF, as well as ΔRDOF, potentially suggesting that additional muscles may be incorporated to produce an avoidance in a flow field background. Over time, the correlation between DA and certain RDOF/ΔRDOF (η, ψ, $\Delta\eta$) became significant during the interquartile range of TOB, while the correlation between DA and χ became insignificant and reached its lowest value during the interquartile range of TOB. Previous studies have found that in response to thermal stimuli, other flight muscles, including M85, M98, M99, M127, showed shifts in bilateral asymmetry similar to M97 (Shoemaker and Robertson, 1998). The participation of these muscles could affect the correlation between M97 DA and RDOF during collision avoidance behaviours as well.

This is the first study to investigate the forewing depressor activity and 3D body movement of loosely-tethered flying locust in response to looming stimuli approaching against different backgrounds. To study physiological mechanisms of behaviour, researchers need to constrain conditions to obtain unambiguous recordings of putative processes. However, animal behaviour usually requires the integration of multiple systems, from sensory input to motor outputs, and thus it is important to investigate the

different levels involved. Previous studies on collision avoidance behaviours mostly focused on the neural level. The few studies that utilized loosely-tethered flying animals were conducted in the wind tunnel, which limited the complexity of visual stimuli that could be projected. With a carefully-designed experimental setup, I better emulated dynamic visual properties of the locust's natural environment. With this setup, the muscular and behavioural data from flying locusts may better reflect how the animal would perform in the natural environment. This could help gain new perspective into this well-studied animal system, and potentially lead to a better understanding of this behaviour. Additionally, the relationship between DA and whole-body behaviours could help build a closed-loop system, and be applied to other animal systems as well.

4.6 FUTURE DIRECTIONS

To fully understand the collision avoidance behaviours of the locusts, it is important to investigate at different levels, i.e., sensory input, motor output, muscle activity, and whole-body behaviour. The presence of a flow field background was shown to modify the DCMD response to looming stimuli (Silva et al., 2015). However, no difference in the response time were found in flying locusts. Further studies would be necessary to investigate how did the locusts process the visual information and interpret it into behavioural outputs.

Since the DCMD recordings were acquired from rigidly-tethered animals, it would be important to record muscle activity from rigidly-tethered animals or, more appropriately, record DCMD from loosely-tethered animals, i.e., comparing neural and EMG data from the same setup, minimizing potential ambiguity from different datasets.

In the current setup, the ringed tether is fixed to the pronotum of the locust. I have drafted a design of a neck collar-shaped tether, which could fix the DCMD electrode to the animal's pronotum and connect to the ringed tether on the dorsal side. In this way, the vibration induced by locust flight could be minimized by having the electrode moving with the locust, while the weight of the electrodes could be counter balanced along with the tether. This would enable simultaneous recordings from DCMD, muscle and behaviour, which could provide multilevel data acquired under the same conditions.

Additional investigation into the potential handedness would be useful in interpreting putative directional bias observed in this and other experiments (Osorio, 1986; Rind, 1990a; Rind, 1990b). If the handedness exists in locusts, it could be part of an effective strategy to maneuvering within complex visual environment. For example, if a large swarm of locusts are migrating together, individual preference of going to a certain side could reduce the chance of collision with conspecifics. To study this, we could project visual stimuli approaching from different sides to a large number of loosely-tethered locusts. The trials with the same visual stimulus could be pooled to determine if there is difference in the M97 firing rate. This experiment could be conducted in the wind tunnel to reduce the effect of corrective steering.

REFERENCES

Anstey, M. L., Rogers, S. M., Ott, S. R., Burrows, M. and Simpson, S. J. (2009). Serotonin mediates behavioral gregarization underlying swarm formation in desert locusts. *Science (80-.).* **323**, 627–630.

Baker, P. S. (1979). The wing movements of flying locusts during steering behaviour. *J. Comp. Physiol. A* **131**, 49–58.

Baker, P. S., Gewecke, M. and Cooter, R. J. (1981). The natural flight of the migratory locust, *Locusta migratoria L.* - III. Wing-beat frequency, flight speed and attitude. *J. Comp. Physiol. A* **141**, 233–237.

Bate, C. M. (1976). Pioneer neurones in an insect embryo. *Nature* **260**, 54–56.

Beĭ-Bienko, G. I. and Mishchenko, L. L. (1963). *Locusts and grasshoppers of the USSR and adjacent countries*. Israel Program for Scientific Translations.

Benaragama, I. and Gray, J. R. (2014). Responses of a pair of flying locusts to lateral looming visual stimuli. *J. Comp. Physiol. A* **200**, 723–738.

Bennett, R. R., Tunstall, J. and Horridge, G. A. (1967). Spectral sensitivity of single retinula cells of the locust. *Z. Vgl. Physiol.* **55**, 195–206.

Bottjer, S., Miesner, E. and Arnold, A. (1984). Forebrain lesions disrupt development but not maintenance of song in passerine birds. *Science (80-.).* **224**, 901–903.

Burrows, M. (1973). Physiological and morphological properties of the metathoracic common inhibitory neuron of the locust. *J. Comp. Physiol.* **82**, 59–78.

Burrows, M. (1996). *The neurobiology of an insect brain*. Oxford University Press on Demand.

Burrows, M. and Fraser Rowell, C. H. (1973). Connections between descending visual interneurons and metathoracic motoneurons in the locust. *J. Comp. Physiol.* **85**, 221–234.

Chan, R. W. and Gabbiani, F. (2013). Collision-avoidance behaviors of minimally restrained flying locusts to looming stimuli. *J. Exp. Biol.* **216**, 641–655.

Chapman, R. F. (1959). Observations on the flight activity of the red locust, *Nomadacris septemfasciata* (Serville). *Behaviour* **14**, 300–334.

Clynen, E., Baggerman, G., Veelaert, D., Cerstiaens, A., Van Der Horst, D., Harthoorn, L., Derua, R., Waelkens, E., De Loof, A. and Schoofs, L. (2001). Peptidomics of the pars intercerebralis-corpus cardiacum complex of the migratory locust, *Locusta migratoria*. *Eur. J. Biochem.* **268**, 1929–1939.

Cohen, J. (1988). *Statistical power analysis for the behavioural sciences Lawrence Earlbaum Associates*. NJ: Hillsdale.

Coombs, S. (1999). Signal detection theory, lateral-line excitation patterns and prey capture behaviour of mottled sculpin. *Anim. Behav.* **58**, 421–430.

Coro, F. and Perez, M. (1983). Peripheral interaction in the tympanic organ of a moth. *Naturwissenschaften* **70**, 99–100.

Dawson, J., Dawson-Scully, K., Robert, D., Robertson and Yacute (1997). Forewing asymmetries during auditory avoidance in flying locusts. *J. Exp. Biol.* **200**, 2323–

2335.

Dawson, J. W., Leung, F.-H. and Robertson, R. M. (2004). Acoustic startle/escape reactions in tethered flying locusts: motor patterns and wing kinematics underlying intentional steering. *J. Comp. Physiol. A* **190**, 581–600.

Dick, P. C. and Gray, J. R. (2014). Spatiotemporal stimulus properties modulate responses to trajectory changes in a locust looming-sensitive pathway. *J. Neurophysiol.* **111**, 1736–1745.

Dick, P. C., Michel, N. L. and Gray, J. R. (2017). Complex object motion represented by context-dependent correlated activity of visual interneurones. *Physiol. Rep.* **5**, e13355.

Dijkgraaf, S. (1963). The function and significance of the lateral-line organs. *Biol. Rev.* **38**, 51–105.

Fotowat, H., Harrison, R. R. and Gabbiani, F. (2011). Multiplexing of motor information in the discharge of a collision detecting neuron during escape behaviors. *Neuron* **69**, 147–158.

Gabbiani, F., Krapp, H. G. and Laurent, G. (1999). Computation of object approach by a wide-field, motion-sensitive neuron. *J. Neurosci.* **19**, 1122–41.

Gabbiani, F., Mo, C. and Laurent, G. (2001). Invariance of angular threshold computation in a wide-field looming-sensitive neuron. *J. Neurosci.* **21**, 314–329.

Gabbiani, F., Krapp, H. G., Koch, C. and Laurent, G. (2002). Multiplicative computation in a visual neuron sensitive to looming. *Nature* **420**, 320–324.

Gaten, E., Huston, S. J., Dowse, H. B. and Matheson, T. (2012). Solitary and gregarious locusts differ in circadian rhythmicity of a visual output neuron. *J. Biol. Rhythms* **27**, 196–205.

Gewecke, M. and Hou, T. (1993). Visual brain neurons in *Locusta migratoria*. In *Sensory Systems of Arthropods (Wiese K, Gribakin FG, Popov AV, Renninger G, eds)*, pp. 119–144.

Gewecke, M., Kirschfeld, K. and Feiler, R. (1990). Identification of optic lobe neurons of locusts by video films. *Biol. Cybern.* **63**, 411–420.

Gray, J. R. (2005). Habituated visual neurons in locusts remain sensitive to novel looming objects. *J. Exp. Biol.* **208**, 2515–2532.

Gray, J. R., Lee, J. K. and Robertson, R. M. (2001). Activity of descending contralateral movement detector neurons and collision avoidance behaviour in response to head-on visual stimuli in locusts. *J. Comp. Physiol. A* **187**, 115–129.

Gray, J. R., Pawlowski, V. and Willis, M. a (2002). A method for recording behavior and multineuronal CNS activity from tethered insects flying in virtual space. *J. Neurosci. Methods* **120**, 211–223.

Greenberg, B. and Noble, G. K. (1944). Social behavior of the American chameleon (*Anolis carolinensis* Voigt). *Physiol. Zool.* **17**, 392–439.

Griffin, D. R., Webster, F. A. and Michael, C. R. (1960). The echolocation of flying insects by bats. *Anim. Behav.* **8**, 141–154.

Grillner, S. (1985). Neurobiological bases of rhythmic motor acts in vertebrates. *Science*

(80-.). **228**, 143–149.

Guest, B. B. and Gray, J. R. (2006). Responses of a looming-sensitive neuron to compound and paired object approaches. *J. Neurophysiol.* **95**, 1428–1441.

Hatsopoulos, N., Gabbiani, F. and Laurent, G. (1995). Elementary computation of object approach by a wide-field visual neuron. *Science (80-.).* **270**, 1000–1003.

Hedwig, B. and Becher, G. (1998). Forewing movements and intracellular motoneurone stimulation in tethered flying locusts. *J. Exp. Biol.* **201 (Pt 12**, 731–44.

Helbling, E. F. and Wood, R. (2017). A Review of propulsion, power, and pontrol architectures for insect-scale flapping-wing vehicles. *Appl. Mech. Rev.* **70**, 1–9.

Hess, C. W. (2008). Walter R. Hess (17.3.1881-12.8.1973). *Schweizer Arch. für Neurol. und Psychiatr.* **159**, 255–261.

Hoekstra, D. and Janssen, J. (1985). Non-visual feeding behavior of the mottled sculpin, *Cottus bairdi*, in Lake Michigan. *Environ. Biol. Fishes* **12**, 111–117.

Horridge, G. A. (1978). The separation of visual axes in apposition compound eyes. *Philos. Trans. R. Soc. B Biol. Sci.* **285**, 1–59.

Huber, F. (1962). Central nervous control of sound production in crickets and some speculations on its evolution. *Evolution (N. Y).* **16**, 429–442.

Ingle, D. (1973). Two visual systems in the frog. *Science (80-.).* **181**, 1053–1055.

James, A. C. and Osorio, D. (1996). Characterisation of columnar neurons and visual signal processing in the medulla of the locust optic lobe by system identification techniques. *J. Comp. Physiol. A* **178**, 183–199.

Jenssen, T. A. (1971). Display analysis of *Anolis nebulosus* (Sauria, Iguanidae). *Copeia* **1971**, 197.

Judge, S. and Rind, F. (1997). The locust DCMD, a movement-detecting neurone tightly tuned to collision trajectories. *J. Exp. Biol.* **200**, 2209–16.

Kennedy, J. S. (1951). The migration of the desert locust (*Schistocerca gregaria Forsk.*). I. The behaviour of swarms. II. A theory of long-range migrations. *Philos. Trans. R. Soc. B Biol. Sci.* **235**, 163–290.

King, J. R. and Comer, C. M. (1996). Visually elicited turning behavior in *Rana pipiens*: comparative organization and neural control of escape and prey capture. *J. Comp. Physiol. A* **178**, 293–305.

Korzan, W. J., Summers, T. R. and Summers, C. H. (2000). Monoaminergic activities of limbic regions are elevated during aggression: Influence of sympathetic social signaling. *Brain Res.* **870**, 170–178.

Krapp, H. G. and Gabbiani, F. (2005). Spatial distribution of inputs and local receptive field properties of a wide-field, looming sensitive neuron. *J. Neurophysiol.* **93**, 2240–2253.

Latchininsky, A. V, Sergeev, M. G., Childebaev, M. K., Chernyakhovsky, M. E., Lockwood, J. A., Kambulin, V. E. and Gapparov, F. A. (2002). Acridids of Kazakhstan, central Asia and adjacent territories. *Assoc. Appl. Acridology Int.*

Linnaeus, C. (1758). *Systema Naturae, edition 10 (Holmiae).*

Loughton, B. G. and Orchard, I. (1981). The nature of the hyperglycaemic factor from

the glandular lobe of the corpus cardiacum of *Locusta migratoria*. *J. Insect Physiol.* **27**, 383–385.

McMillan, G. and Gray, J. R. (2012). A looming-sensitive pathway responds to changes in the trajectory of object motion. *J. Neurophysiol.* **108**, 1052–1068.

McMillan, G. A. and Gray, J. R. (2015). Burst firing in a motion-sensitive neural pathway correlates with expansion properties of looming objects that evoke avoidance behaviors. *Front. Integr. Neurosci.* **9**, 60.

McMillan, G. a, Loessin, V. and Gray, J. R. (2013). Bilateral flight muscle activity predicts wing kinematics and 3-dimensional body orientation of locusts responding to looming objects. *J. Exp. Biol.* **216**, 3369–80.

Meldrum Robertson, R. (1986). Neuronal circuits controlling flight in the locust: central generation of the rhythm. *Trends Neurosci.* **9**, 278–280.

Mello, C., Nottebohm, F. and Clayton, D. (1995). Repeated exposure to one song leads to a rapid and persistent decline in an immediate early gene's response to that song in zebra finch telencephalon. *J. Neurosci.* **15**, 6919–25.

Miall, R. C. (1978). The flicker fusion frequencies of six laboratory insects, and the response of the compound eye to mains fluorescent "ripple." *Physiol. Entomol.* **3**, 99–106.

Mishchenko, L. L. (1952). Fauna of the USSR. *Insects: Orthoptera* **4**,.

Möhl, B. and Zarnack, W. (1977). Activity of the direct downstroke flight muscles ofLocusta migratoria (L.) during steering behaviour in flight. *J. Comp. Physiol. A*

118, 235–247.

Mohr, N. A. and Gray, J. R. (2003). Collision avoidance responses in loosely tethered flying locusts. In *Neurosci Abstr*, .

Moshtagh, N. (2005). Minimum volume enclosing ellipsoids. *Convex Optim.* 1–9.

Nottebohm, F., Stokes, T. M. and Leonard, C. M. (1976). Central control of song in the canary, *Serinus canarius*. *J. Comp. Neurol.* **165**, 457–486.

O'Shea, M. and Williams, J. L. D. (1974). The anatomy and output connection of a locust visual interneurone; the lobular giant movement detector (LGMD) neurone. *J. Comp. Physiol.* **91**, 257–266.

O'Shea, M., Rowell, C. H. F. and Williams, J. L. D. (1974). The anatomy of a locust visual interneurone; the descending contralateral movement detector. *J. Exp. Biol.* **60**, 1–12.

Ong, M., Bulmer, M., Groening, J. and Srinivasan, M. V. (2017). Obstacle traversal and route choice in flying honeybees: Evidence for individual handedness. *PLoS One* **12**,.

Orlovskiĭ, G. N., Deliagina, T. G. and Grillner, S. (1999). *Neuronal control of locomotion: from mollusc to man*. New York: Oxford University Press.

Osorio, D. (1986). Directionally selective cells in the locust medulla. *J. Comp. Physiol. A* **159**, 841–847.

Parkinson, R. H., Little, J. M. and Gray, J. R. (2017). A sublethal dose of a neonicotinoid insecticide disrupts visual processing and collision avoidance

behaviour in Locusta migratoria. *Sci. Rep.* **7**, 936.

Pener, M. P. and Yerushalmi, Y. (1998). The physiology of locust phase polymorphism: An update. *J. Insect Physiol.* **44**, 365–377.

Rayner, J. M. V (1988). Form and function in avian flight. *Curr. Ornithol.* **5**, 1–66.

Ribak, G., Rand, D., Weihs, D. and Ayali, A. (2012). Role of wing pronation in evasive steering of locusts. *J. Comp. Physiol. A* **198**, 541–555.

Rind, F. C. (1984). A chemical synapse between two motion detecting neurones in the locust brain. *J. Exp. Biol.* **110**, 143–167.

Rind, F. C. (1987). Non-directional, movement sensitive neurones of the locust optic lobe. *J. Comp. Physiol. A* **161**, 477–494.

Rind, F. C. (1990a). A directionally selective motion-detecting neurone in the brain of the locust: physiological and morphological characterization. *J. Exp. Biol.* **19**, 1–19.

Rind, F. (1990b). Identification of directionally selective motion-detecting neurones in the locust lobula and their synaptic connections with an identified descending neurone. *J. Exp. Biol.* **149**, 21–43.

Rind, F. C. and Simmons, P. J. (1992). Orthopteran DCMD neuron: a reevaluation of responses to moving objects. I. Selective responses to approaching objects. *J. Neurophysiol.* **68**, 1654–66.

Robertson, R. M. and Johnson, a G. (1993). Collision avoidance of flying locusts: steering torques and behaviour. *J. Exp. Biol.* **183**, 35–60.

Robertson, R. M. and Pearson, K. G. (1983). Interneurons in the flight system of the

locust: Distribution, connections, and resetting properties. *J. Comp. Neurol.* **215**, 33–50.

Robertson, R. M. and Reye, D. N. (1992). Wing movements associated with collision-avoidance manoeuvres during flight in the locust *Locusta migratoria*. *J. Exp. Biol.* **163**, 231–258.

Robertson, R., Kuhnert, C. and Dawson, J. (1996). Thermal avoidance during flight in the locust *Locusta migratoria*. *J. Exp. Biol.* **199**, 1383–93.

Roeder, K. D. and Treat, A. E. (1957). Ultrasonic reception by the tympanic organ of noctuid moths. *J. Exp. Zool.* **134**, 127–157.

Rogers, S. M., Matheson, T., Despland, E., Dodgson, T., Burrows, M. and Simpson, S. J. (2003). Mechanosensory-induced behavioural gregarization in the desert locust *Schistocerca gregaria*. *J. Exp. Biol.* **206**, 3991–4002.

Rovainen, C. M. (1974). Synaptic interactions of identified nerve cells in the spinal cord of the sea lamprey. *J. Comp. Neurol.* **154**, 189–206.

Rowell, C. H. F. (1971). The orthopteran descending movement detector (DMD) neurones: a characterisation and review. *Z. Vgl. Physiol.* **73**, 167–194.

Rowell, C. H. and O'Shea, M. (1976). The neuronal basis of a sensory analyser, the acridid movement detector system. I. Effects of simple incremental and decremental stimuli in light and dark adapted animals. *J. Exp. Biol.* **65**, 273–88.

Santer, R. D. (2006). Role of an identified looming-sensitive neuron in triggering a flying locust's escape. *J. Neurophysiol.* **95**, 3391–3400.

Santer, R. D., Simmons, P. J. and Rind, F. C. (2005). Gliding behaviour elicited by lateral looming stimuli in flying locusts. *J. Comp. Physiol. A* **191**, 61–73.

Schlotterer, G. R. (1977). Response of the locust descending movement detector neuron to rapidly approaching and withdrawing visual stimuli. *Can. J. Zool.* **55**, 1372–1376.

Schnitzler, H.-U. and Flieger, E. (1983). Detection of oscillating target movements by echolocation in the Greater Horseshoe bat. *J. Comp. Physiol. A* **153**, 385–391.

Schoofs, L., Holman, G. M., Paemen, L., Veelaert, D., Amelinckx, M. and De Loof, A. (1993). Isolation, identification and synthesis of PDVDHFLRFamide (SchistoFLRFamide) in *Locusta migratoria* and its association with the male accessory glands, the salivary glands, the heart, and the oviduct. *Peptides* **14**, 409–421.

Shoemaker, K. L. and Robertson, R. M. (1998). Flight motor patterns of locusts responding to thermal stimuli. *J. Comp. Physiol. A* **183**, 477–488.

Silva, A. C., Silva, J. and Santos, C. P. (2012). LGMD based neural network for automatic collision detection. In *Proc ICINCO*, pp. 132–140.

Silva, A. C., McMillan, G. A., Santos, C. P. and Gray, J. R. (2015). Background complexity affects the response of a looming-sensitive neuron to object motion. *J. Neurophysiol.* 218–231.

Simmons, P. J. (1980). Connexions between a movement-detecting visual interneurone and flight motoneurones of a locust. *J. Exp. Biol.* **86**, 87–97.

Simmons, P. J. and Rind, F. C. (1992). Orthopteran DCMD neuron: a reevaluation of

responses to moving objects. II. Critical cues for detecting approaching objects. *J. Neurophysiol.* **68**, 1667–82.

Simmons, P. J., Rind, F. C. and Santer, R. D. (2010). Escapes with and without preparation: The neuroethology of visual startle in locusts. *J. Insect Physiol.* **56**, 876–883.

Simpson, S. J., Despland, E., Hagele, B. F. and Dodgson, T. (2001). Gregarious behavior in desert locusts is evoked by touching their back legs. *Proc. Natl. Acad. Sci. U. S. A.* **98**, 3895–3897.

Simpson, S. J., McCaffery, A. R. and Hägeke, B. F. (2007). A behavioural analysis of phase change in the desert locust. *Biol. Rev.* **74**, 461–480.

Straw, A. D. (2008). Vision Egg: An open-source library for realtime visual stimulus generation. *Front. Neuroinform.* **2**, 1–10.

Summers, C. H. and Greenberg, N. (1995). Activation of central biogenic amines following aggressive interaction in male lizards, *Anolis carolinensis*. *Brain. Behav. Evol.* **45**, 339–349.

Tsyplenkov, Y. P. (1970). Grasshoppers (Orthoptera, Acridoidea) of the Korean Peoples' Republic. *Entomol. Rev.*

Uvarov, B. P. (1966). *Grasshoppers and locusts: A handbook of general acridology. Vol. 1. Anatomy, physiology, development, phase polymorphism, introduction to taxonomy*. Published for the Anti-Locust Research Centre at the University Press.

Uvarov, B. P. (1977). *Grasshoppers and locusts: A handbook of general acridology. Vol.*

2. Behaviour, ecology, biogeography, population dynamics. Centre for Overseas Pest Research.

Vater, M., Casseday, J. H. and Covey, E. (1995). Convergence and divergence of ascending binaural and monaural pathways from the superior olives of the mustached bat. *J. Comp. Neurol.* **351**, 632–646.

Vinay, L., Barthe, J. Y. and Grillner, S. (1996). Central modulation of stretch receptor neurons during fictive locomotion in lamprey. *J. Neurophysiol.* **76**, 1224–1235.

von Holst, E. (1939). The behavioral physiology of man and animals. *Collect. Pap. Erich von Holst*.

Waloff, Z. (1972). Orientation of flying locusts, Schistocerca gregaria (Forsk.), in migrating swarms. *Bull. Entomol. Res.* **62**, 1.

Waters, D. (1996). The peripheral auditory characteristics of noctuid moths: information encoding and endogenous noise. *J. Exp. Biol.* **199**, 857–868.

Wendler, G. (1974). The influence of proprioceptive feedback on locust flight co-ordination. *J. Comp. Physiol.* **88**, 173–200.

White, L. (1961). Eilmer of Malmesbury, an eleventh century aviator: a case study of technological innovation, its context and tradition. *Technol. Cult.* **2**, 97.

Wilson, D. M. (1961). The central nervous control of flight in a locust. *J. Exp. Biol.* **38**, 471–490.

Wilson, D. M. (1968). The nervous control of insect flight and related behavior. In *Advances in Insect Physiology*, pp. 289–338.

Wilson, M. (1975). Angular sensitivity of light and dark adapted locust retinula cells. *J. Comp. Physiol. A* **97**, 323–328.

Wilson, M. (1978). The functional organisation of locust ocelli. *J. Comp. Physiol. A* **124**, 297–316.

Wilson, D. M. and Weis-Fogh, T. (1962). Patterned activity of co-Ordinated motor units , studied in flying locusts. *J. Exp. Biol.* **39**, 643–667.

Zarnack, W. (1988). The effect of forewing depressor activity on wing movement during locust flight. *Biol. Cybern.* **59**, 55–70.

Zupanc, G. (2010). *Behavioral neurobiology: an integrative approach*. Oxford University Press.